Biogeosciences Discuss., doi:10.5194/bg-2016-169, 2016
Manuscript under review for journal Biogeosciences
Published: 18 May 2016

Biogeosciences Discussions
Open Access
EGU

A cobalt plume in the oxygen minimum zone of the Eastern Tropical South Pacific

N. J. Hawco,[1,2] D.C. Ohnemus,[3] J. A. Resing,[4] B. S. Twining[3] and M. A. Saito[2]

[1] MIT/WHOI Joint Program in Oceanography/Applied Ocean Science and Engineering, Woods Hole, MA, USA
[2] Department of Marine Chemistry and Geochemistry, Woods Hole Oceanographic Institution, Woods Hole, MA, USA
[3] Bigelow Laboratory for Ocean Sciences, East Boothbay, ME, USA
[4] Joint Institute for the Study of the Atmosphere and the Ocean, University of Washington and NOAA-PMEL, Seattle, WA, USA

Correspondence to: M. A. Saito (msaito@whoi.edu)

Biogeosciences Discuss., doi:10.5194/bg-2016-169, 2016
Manuscript under review for journal Biogeosciences
Published: 18 May 2016

Abstract. Cobalt is a nutrient to phytoplankton, but knowledge about its biogeochemical cycling is limited, especially in the Pacific Ocean. Here, we report sections of dissolved cobalt and labile cobalt from the US GEOTRACES GP16 transect in the South Pacific. The cobalt distribution is closely tied to the extent and intensity of the oxygen minimum zone in the eastern South Pacific with highest concentrations measured at the oxycline near the Peru margin. Below 200 m, remineralization and circulation produce an inverse relationship between cobalt and dissolved oxygen that extends throughout the basin. Within the oxygen minimum zone, elevated concentrations of labile cobalt are generated by input from coastal sources and reduced scavenging at low O_2. As these high cobalt waters are upwelled and advected offshore, phytoplankton export returns cobalt to low-oxygen water masses underneath. West of the Peru upwelling region, dissolved cobalt is less than 10 pM in the euphotic zone and strongly bound by organic ligands. Because the cobalt nutricline within the South Pacific gyre is deeper than oligotrophic regions in the North and South Atlantic, cobalt involved in sustaining phytoplankton productivity in the gyre is heavily recycled and ultimately arrives from lateral transport of upwelled waters from the eastern margin. In contrast to large coastal inputs, hydrothermal vents along the Eastern Pacific Rise appear to be a minor source of cobalt. Overall, these results demonstrate that oxygen biogeochemistry exerts a strong influence on cobalt cycling.

Keywords. Cobalt, oxygen minimum zone, scavenging, GEOTRACES, hydrothermal vents, manganese oxides, phytoplankton, South Pacific, Peru Upwelling, micronutrient

1. Introduction

Cobalt is the least abundant inorganic nutrient in seawater and its scarcity may affect phytoplankton growth in certain regions (Moore et al., 2013). In the high macronutrient waters of the Costa Rica upwelling dome, for instance, Co and iron (Fe) amendments to surface seawater increased phytoplankton production more than Fe alone, promoting growth of the cyanobacterium *Synechococcus* (Ahlgren et al., 2014; Saito et al., 2005). While eukaryotic phytoplankton mainly use cobalt to compensate for insufficient zinc (Sunda and Huntsman, 1995), populating the same enzymes with either metal (Yee and Morel, 1996), marine cyanobacteria have an absolute growth requirement for Co that cannot be substituted and suggests they may be more prone to limitation (Saito et al., 2002). Yet, the extent to which their

Biogeosciences Discuss., doi:10.5194/bg-2016-169, 2016
Manuscript under review for journal Biogeosciences
Published: 18 May 2016

growth *in situ* is affected by cobalt scarcity ultimately depends on the processes that add Co to, or remove it from, the surface ocean relative to other limiting nutrients.

Biological cycling of dissolved cobalt (dCo) is apparent in vertical profiles, showing uptake and export in the surface and regeneration in the thermocline (Bown et al., 2011; Dulaquais et al., 2014a; Noble et al., 2012). While dCo in the euphotic zone can be entirely bound by strong organic ligands, a substantial portion of subsurface dCo is unbound and labile (10–50 %, Bown et al., 2012; Ellwood and van den Berg, 2001; Saito and Moffett, 2001; Saito et al., 2005) and therefore vulnerable to scavenging (Moffett and Ho, 1996). The similar ionic radii and redox potentials of cobalt and manganese (Mn) cause dCo to be actively incorporated into bacterial Mn-oxides, which sink from the water column and accumulate in marine sediments (Cowen and Bruland, 1985; Moffett and Ho, 1996; Swanner et al., 2014). Below the euphotic zone, the persistence of labile cobalt (LCo) throughout the Atlantic indicates that scavenging of dCo, unlike Fe, is slow (Noble et al., 2012). On timescales of ocean circulation, however, scavenging is responsible for decreasing dCo concentrations with depth and for the low ratio between dCo and macronutrients in deep waters (Moore et al., 2013). As these deep waters are repackaged into thermocline water masses and eventually brought to the surface (Sarmiento et al., 2011), the upper ocean would become depleted in cobalt – as well as other hybrid metals like Fe – without external sources that keep pace with scavenging (Bruland and Lohan, 2003; Noble et al., 2008).

Yet, the nature of marine cobalt sources is uncertain. In zonal sections of the North and South Atlantic, sources appear to be concentrated along continental margins (Noble and Saito, in prep; Noble et al., 2012). In the western Atlantic, dCo concentrations exceeding 100pM were

Biogeosciences Discuss., doi:10.5194/bg-2016-169, 2016
Manuscript under review for journal Biogeosciences
Published: 18 May 2016

89 associated with the flow of Upper Labrador Seawater, likely gained through intense sediment
90 resuspension along the shelf or input prior to subduction (Noble and Saito, In prep). dCo in fresh
91 and estuarine waters can be 100–1000x greater than seawater (Gaillardet et al., 2003; Knauer et
92 al., 1982; Tovar-Sánchez et al., 2004) and terrigenous inputs from the American continent can be
93 clearly seen in lower salinity surface waters influenced by the Gulf Stream (Noble and Saito, in
94 prep; Saito and Moffett, 2002) and Amazon discharge (Dulaquais et al., 2014b). Yet, in both the
95 North and South Atlantic, a much larger dCo plume was associated with the oxygen minimum
96 zones along the Mauritanian and Namibian coasts (Noble and Saito, in prep, Noble et al., 2012).
97 Although these waters are not anoxic, the dCo plumes imply that O_2 over the continental shelf is
98 sufficiently low that reductive dissolution of Mn and Fe oxides in sediments releases a large flux
99 of dCo to the water column (Heggie and Lewis, 1984; Sundby et al., 1986). Drawing from large
100 inventories in the Atlantic OMZs, upwelling along eastern margins provides a large dCo flux to
101 the surface ocean. While surface dCo maxima from atmospheric deposition generally do not
102 appear in vertical profiles, this process may be important for regions that are isolated from
103 continental input or receive very high levels of dust (e.g. the Sargasso Sea, Dulaquais et al.,
104 2014a; Shelley et al., 2012).
105
106 To date, sectional datasets for dCo have been confined to the Atlantic and, as such, our
107 understanding of cobalt cycling may be biased by the dominant processes occurring there. In
108 comparison, the South Pacific receives considerably less dust deposition and river input
109 (Mahowald et al., 2005; Milliman and Farnsworth, 2011), but hosts a much larger and more
110 reducing oxygen minimum zone. Surface transects off Peru and the Costa Rica Dome suggest a
111 large source from upwelling (Ahlgren et al., 2014; Saito et al., 2004, 2005); however, profiles in

Biogeosciences Discuss., doi:10.5194/bg-2016-169, 2016
Manuscript under review for journal Biogeosciences
Published: 18 May 2016

the tropical Pacific are sparse (Noble et al., 2008; Saito et al., 2014). We measured dissolved and labile cobalt concentrations from over 750 samples collected onboard the 2013 US GEOTRACES GP16 expedition across the South Pacific along 12° S, intersecting coastal upwelling along the Peru margin, hydrothermal venting over the East Pacific rise, and oligotrophic conditions near Polynesia (Fig. 1). Across this section, the distribution of dCo and LCo follow the intensity of the oxygen minimum zone, with highest concentrations near the South American shelf and low concentrations in both deep waters and oligotrophic surface waters, matching OMZ-associated plumes observed in the Atlantic.

2. Methods

2.1 Sample collection and handling

Sampling on GP16 was conducted with a 24 position trace metal clean titanium rosette attached to a non-metallic Kevlar cable designed for the U.S. GEOTRACES program (Cutter and Bruland, 2012). An additional sample was collected from a surface towfish at each station. Subsamples were collected in a Class-100 sampling van from 12 L Go-Flo bottles (General Oceanics) and passed through 0.2 μM Acropack filters (Pall). All bottles were rinsed 3x with sample seawater before being filled entirely, leaving no headspace. For samples analyzed at sea, both dissolved and labile cobalt were analyzed from the same bottle. All samples were kept refrigerated at 4° C until analysis in a HEPA filtered clean van. All of the LCo samples and more than 90 % of dCo samples were analyzed at sea. Samples not analyzed at sea were preserved for dCo immediately after sampling using metal-free gas adsorbing satchels (Mitsubishi Gas Chemical, model RP-3K), using 3–4 satchels per 6 seawater samples. Gas-impermeable plastic

Biogeosciences Discuss., doi:10.5194/bg-2016-169, 2016
Manuscript under review for journal Biogeosciences
Published: 18 May 2016

bags (Ampac) were heat sealed and were hand carried directly to Woods Hole at 4° C following disembarkation.

2.2 Cobalt determination by cathodic stripping voltammetry

dCo and LCo were measured using a cathodic stripping voltammetry (CSV) method optimized for organic speciation by Saito and Moffett, 2001. This method relies on the complexation of inorganic Co species by a strong synthetic ligand, dimethylglyoxime (DMG, $K^{cond} = 10^{11.5\pm0.3}$), which forms a bis-complex, $Co(DMG)_2$, with Co^{2+} that readily absorbs to a hanging mercury drop (Saito and Moffett, 2001). The $Co(DMG)_2$ complex is measured following a fast, 10V s^{-1} sweep that reduces both the Co (II) to Co(0) and the DMG to 2,3-bis(hydroxylamino)butane, producing an 8 – 10 electron decrease in current for each $Co(DMG)_2$ complex (Baxter et al., 1998). The height of the $Co(DMG)_2$ reduction peak at -1.15 V is measured is directly proportional to the Co concentration.

Triplicate scans of the seawater sample were followed by four standard cobalt additions (25 pM per addition) and the slope of their linear regression (mean $R^2 = 0.998$) was used to calculate the sample specific sensitivity (in nA pM^{-1}). The cobalt concentration was determined by dividing the mean of the three baseline peaks by the sensitivity, and correcting for reagent volume. The average deviation for these triplicate scans was 1.5 pM.

dCo analyses were conducted after a 1-hour UV oxidation procedure to remove strong organic ligands that prevent Co binding by DMG. UV digestion was performed in 15 mL quartz glass tubes using a Metrohm 705 UV digester (Metrohm USA). Temperature was maintained below

Biogeosciences Discuss., doi:10.5194/bg-2016-169, 2016
Manuscript under review for journal Biogeosciences
Published: 18 May 2016

20° C to minimize evaporation losses. After UV digestion, 11 mL of sample was pipetted into 15mL polypropylene tubes and DMG and a buffering agent, EPPS, were added to final concentrations of 400µM and 3.8mM, respectively. 8.5 mL of sample solution was added to a Teflon analysis cup and mixed with 1.5 mL 1.5M $NaNO_2$, making a final analysis volume of 10 mL.

LCo was measured after >8 hour incubation of 11 mL of seawater with 400 µM DMG in a Teflon cup. LCo is therefore the concentration that will readily exchange with DMG. After this time, the sample was poured into an autosampler-compatible 15 mL poly-propylene tube (separate from those used for dCo analyses) and EPPS was added to 3.8 mM.

2.2.1 Preparing reagent and blanks

All bottles and sample tubes were soaked for >1 week in the acidic detergent Citranox, rinsed thoroughly with Milli-Q water (Millipore), filled with 10 % trace metal grade HCl (J.T. Baker) to soak for 10 days, and rinsed thoroughly with ~10 mM TM-grade HCl. DMG (Sigma-Aldrich) was purified by recrystallization in a 1 mM EDTA solution (Sigma-Aldrich). Crystals were filtered, dried, and dissolved in HPLC grade methanol to a concentration of 0.1 M (Saito and Moffett, 2001). EPPS (Fischer) and Sodium Nitrite (Millipore) were both dissolved in Milli-Q water to 0.5 M and 1.5 M, respectively, and treated with separate batches of thoroughly cleaned Chelex-100 beads (Bio-Rad) to remove background Co and Ni (Price et al., 1989). Standard additions were generated by diluting a 1 ppm certified reference standard (SPEX Certiprep) with 10 mM HCl to a concentration of 5.00 nM. 50 µl of this solution was added to the 10mL sample volume for each standard addition (25 pM addition).

Biogeosciences Discuss., doi:10.5194/bg-2016-169, 2016
Manuscript under review for journal Biogeosciences
Published: 18 May 2016

180

181 To determine reagent blanks, Co-free seawater was generated by treating UV-seawater with
182 cleaned Chelex-100 beads. The seawater was then UV digested a second time to remove any
183 ligands leached during Chelex treatment. Any dCo measured in the Chelexed seawater derives
184 from addition of Co from analytical reagents. The mean blank for at sea analysis was
185 consistently low, 3.7 ± 1.2 pM (n=28). For analyses at Woods Hole, mean blank was 4.7 ± 1.4
186 pM (n=12). Blanks were subtracted from all measured values. Detection limits were calculated
187 as triple the standard deviation of the blank: 3.6 pM for at-sea analyses and 4.2 pM for samples
188 measured in Woods Hole.

189

190 **2.2.2 Automated cobalt analyses**

191 To accommodate a greater number of samples, our previous workflow (Noble et al., 2008) was
192 modified to incorporate fully automated sample analyses using the Metrohm 837 Sample
193 Processor autosampler. All measurements were performed using an Eco-Chemie μAutolabIII
194 system connected to a Metrohm 663 VA stand. A hanging drop mercury electrode (Metrohm)
195 was set to semi-hanging drop mode and accompanied by a 3M KCl/AgCl reference electrode and
196 glassy carbon auxiliary electrode. Scheduling and data acquisition were controlled using NOVA
197 1.8 software (Metrohm Autolab B.V). Automated delivery of seawater, sodium nitrite, and Co
198 standard to the analysis cup was accomplished by three dedicated Dosino 800 burettes
199 (Metrohm). Sample volume was increased to allow ~2 mL for conditioning tubing and analysis
200 cup prior of sample delivery.

201

Biogeosciences Discuss., doi:10.5194/bg-2016-169, 2016
Manuscript under review for journal Biogeosciences
Published: 18 May 2016

Tubes containing 11 mL seawater, DMG, and EPPS were inverted several times and placed onto a sampling rack where 8.5 mL of the mixture was dosed into the Teflon analysis cup. 1.5 mL 1.5 M sodium nitrite was added directly to the sample cup. Samples were purged with high-purity N_2 (>99.99 %) for 180 s and then conditioned for 90 s at -0.6 V. Scan sweeps were run at 10 V s^{-1} from -0.6 V to -1.4 V. Before each analysis, the sample cup was rinsed fully with Milli-Q water and 1 mL sample before measurement. Between uses, autosampler tubes, quartz vials, and Teflon cups were rinsed with 10 mM HCl, Milli-Q water, and 1-2 mL of new sample. The autosampler sample uptake line was rinsed with 10 mM HCl and Milli-Q when transitioning from LCo analyses to dCo analyses.

We noticed a decrease in sensitivity of preserved samples relative to those analyzed at sea, possibly caused by an increase in the sample pH during storage. Sensitivity was restored by doubling the concentration of our buffering agent, EPPS, in the sample to a final concentration of 7.6 mM. We tested a broader range of EPPS additions in UV seawater and found the cobalt concentration unchanged while the deviation between triplicate scans was reduced markedly by the increase in sensitivity (data not shown). We tentatively attribute this decrease in sensitivity in preserved samples to CO_2 adsorption by gas satchels, which would increase sample pH.

2.2.3 Signal processing

Analyses conducted at sea were characterized with a mild to moderate electrical interference that mandated additional processing before peak height could be reliably measured (Fig. 2). We opted for a simplified least squared fitting routine included in the NOVA software package that conducts a 15-point weighted moving average – equivalent to a 36.9 mV analytical window –

Biogeosciences Discuss., doi:10.5194/bg-2016-169, 2016
Manuscript under review for journal Biogeosciences
Published: 18 May 2016

according to a 2nd order polynomial. This method did not distort cobalt concentrations when noise was low (Fig. 2a, b). A small fraction of scans (~3 %) were not adequately fit using this routine and were instead smoothed using a 9-point linear moving average (22.1 mV window, Fig. 2c), also included in NOVA. For all samples, peak height was measured manually to minimize peak distortion due to added noise.

Subsequent analyses in the laboratory at Woods Hole were able to remove this signal by increasing the current sampling step from 2.46 mV (341 points between -0.6V to -1.4V) to 4.88 mV (174 points) which eliminated the need for smoothing prior to sample analysis. We observed good agreement between samples analyzed at sea and in lab, indicating that the smoothing procedures applied at sea did not bias the data and that gas adsorbing satchels preserved original concentrations (Noble and Saito, in prep).

2.2.4 Intercalibration and internal laboratory standard

All data reported in this manuscript have been submitted to the Biological and Chemical Oceanography Data Management Center (BCO-DMO). Our laboratory continues to participate in international intercalibration efforts through the GEOTRACES program in anticipation of the release of the 2nd Intermediate Data Product, Summer 2017. The sampling scheme for GP16 included 2 overlapping samples per full depth profile where the shallowest sample of the deep cast matched the deepest sample for the mid cast and the shallowest sample from the mid cast matched the deepest sample from the shallow cast (i.e. a 36-point profile is composed of 34 discreet depths and 2 overlapping depths). Comparing overlapping samples collected at the same depth and location on separate hydrocasts provides a measure of reproducibility. The average

Biogeosciences Discuss., doi:10.5194/bg-2016-169, 2016
Manuscript under review for journal Biogeosciences
Published: 18 May 2016

248 difference between dCo analyses across 40 overlapping depth samples was 5.7 pM with a
249 median difference of 3.5 pM. For labile cobalt, average deviation was 2.1 pM (median of 2.0
250 pM, n=41). Least-squares regression of these samples yielded slopes close to 1(0.98 for dCo and
251 0.96 for LCo; y-intercept forced to 0), indicating good reproducability. Furthermore,
252 comparisons with other groups measuring dCo in the same samples reported here suggest strong
253 agreement between groups despite major methodological differences (Parker and Bruland,
254 personal communication).
255
256 Because acidified community reference materials such as the SAFe standards require a delicate
257 neutralization to pH 7.5–8 prior to analysis, a large batch of UV oligotrophic seawater was
258 generated prior to the cruise and used to access instrument performance during at sea analysis.
259 This consistency seawater standard was run ~3x per week, as were blanks, and values were
260 stable over several reagent batches for the duration of the cruise (4.5 ± 2.1 pM, n=28). SAFe
261 standard D1 was measured at sea (48.5 ± 2.4 pM, n=3) and fell within 1 SD of the consensus
262 value (46.6 ± 4.8 pM). SAFe standard D2 and GEOTRACES standard GSP were run at higher
263 frequency for analyses at Woods Hole. Our measurements of D2 (46.9 ± 3.0 pM, n=7) agreed
264 with consensus values (45.7 ± 2.9) and concentrations from our lab published previously (Noble
265 et al., 2012). While the GSP standard does not have a consensus value, our determinations (2.5 ±
266 2.0 pM, n=10) are within the range for SAFe S (4.9 ± 1.2 pM), which was collected at the same
267 offshore location as GSP. Acidified SAFe and GEOTRACES standards were neutralized with
268 concentrated ammonium hydroxide (Seastar), mixing the entire sample between drops, prior to
269 UV digestion. When base was added more quickly, measured Co was halved, presumably due to
270 adsorption or co-precipitation onto magnesium hydroxides formed during base addition. For

Biogeosciences Discuss., doi:10.5194/bg-2016-169, 2016
Manuscript under review for journal Biogeosciences
Published: 18 May 2016

271 analysis of neutralized standards, we found a ~6:1 EPPS:NH_4OH (M:M) buffer improved pH
272 stability during analysis and removed significant baseline drift observed with samples solely
273 buffered with EPPS.
274
275 **2.3 Particulate metal analyses**
276 Particulate material collected from Go-Flo bottles was filtered onto acid-cleaned 0.45 µm
277 polyethersulfone filters (25 mm). Digestion protocol and analyses are identical to those used to
278 measure particulate metal concentrations during the North Atlantic GA03 cruise, described in
279 Twining et al. 2015. After filtration, filters were halved, digested at 135° C in sealed Teflon vials
280 containing 4 M HCL, HNO_3, and HF, dried, and redissolved in 0.32M HNO_3 before analysis.
281 pCo, pMn and pP concentrations were measured by ICP-MS (Element 2, Thermo Scientific),
282 calibrated using external multi-element standard curves, and corrected for instrument drift and
283 sample recovery by In and Cs internal standards. More detailed methods for this dataset can be
284 found elsewhere (Ohnemus et al., In Review).
285
286 **3. Results**
287 We report 680 determinations of dissolved cobalt (dCo) and 783 determinations of labile cobalt
288 (LCo) measured at sea, onboard the GP16 expedition in October–December 2013, as well as an
289 additional 140 measurements of dCo measured from preserved samples on land. Throughout the
290 GP16 transect, nutrient uptake and scavenging result in a hybrid-type profile for dCo (Fig. 3),
291 similar to dCo profiles from the Atlantic (Bown et al., 2011; Dulaquais et al., 2014b; Noble et
292 al., 2012; Noble and Saito, in prep) and North Pacific (Ahlgren et al., 2014; Knauer et al., 1982;
293 Saito et al., 2014). dCo ranged from <3 pM (below detection) in the South Pacific Gyre to 210

Biogeosciences Discuss., doi:10.5194/bg-2016-169, 2016
Manuscript under review for journal Biogeosciences
Published: 18 May 2016

294 pM beneath the oxycline near the Peru Margin (Station 1). In the deep Pacific, concentrations
295 fell between 20–40 pM but increased slightly at deepest stations below 4500 m. These values are
296 much less than those observed in zonal transects surveying the North and South Atlantic (Noble
297 et al., 2012; Noble and Saito, in prep) but are similar to measurements in the Southern Ocean
298 (Bown et al., 2011), indicating that dCo is scavenged in the deep ocean along meridional
299 overturing circulation. Below 3000 m, dCo is somewhat lower east of the Eastern Pacific Rise
300 (EPR), and matches less oxygenated, older waters than in the western portion of the transect
301 (Fig. 4). While many profiles west of the EPR show considerable variation between 2000–3000
302 m suggestive of hydrothermal influence, the range is small (<10 pM) relative to background
303 concentrations (30–40 pM) and unlike the 50-fold excess of hydrothermal dFe and dMn above
304 background seawater measured at Station 18 (Resing et al., 2015).
305
306 dCo peaks in the mesopelagic, typically between 300–500 m. Towards the Peru shelf, this
307 maximum shoals and increases, following the position and intensity of the oxygen minimum
308 zone (OMZ, defined here as O_2 < 20 μM). Although the OMZ is several hundred meters thick
309 near the eastern margin (Fig. 3), dCo concentrations >100 pM are restricted to samples collected
310 just below the oxycline. Despite this narrow depth range, dCo >100 pM extends as far as 100°
311 W. For all depths below 200 m, dCo follows a negative linear relationship with O_2 (Fig. 5a).
312 Over the Peru shelf, maximum dCo was measured at the top of the OMZ and dCo decreased with
313 depth (except for the shallowest and most shoreward Station 2). Only at the western edge of the
314 section do dCo and O_2 decouple: the dCo maximum at station 36 is deeper (500–1000 m) than
315 the oxygen minimum (300–500 m), seemingly independent of the influence of the South Pacific
316 OMZ (Fig. 3).

Biogeosciences Discuss., doi:10.5194/bg-2016-169, 2016
Manuscript under review for journal Biogeosciences
Published: 18 May 2016

All profiles show a surface or near-surface minimum that indicates biological uptake and export. As a result, dCo is well traced by dissolved phosphate, PO_4, in the upper 200 m of the ETSP (Fig. 5c). This relationship holds despite sharp transitions to high dCo in the oxycline near the Peru shelf. Upwelling of O_2-depleted, PO_4-rich waters along the eastern boundary results in high surface dCo, decreasing westward due to mixing and export. A secondary surface dCo maximum marked a cyclonic eddy sampled at 89° W (Station 9, V. Sanial, personal communication), which appeared to transport a shelf-like dCo and LCo signature for the upper 300 m into the offshore OMZ (Fig. 6). Toward the South Pacific gyre, dCo in the euphotic zone falls below 10 pM. While the lowest PO_4 was found in low salinity surface waters west of 140° W, minimum dCo and deepest nutriclines corresponded to a southwestward excursion in the transect between Stations 17–23 (109–120° W), which were accompanied by high salinities (>36) associated with the eastern part of the subtropical gyre (Fig. 13). In contrast to the deep, smooth dCo nutricline further to the east, stations at the western edge of the section (Stations 32, 34, and 36) contained 20 pM Co until ~50 m where concentrations decrease sharply surfaceward, resembling profiles in the North Atlantic (Fig. 3; Noble and Saito, in prep).

The surface minimum in dCo is mirrored by a near-surface maximum in particulate cobalt (pCo) from biological uptake throughout the GP16 section. The distribution of pCo (Fig. 6c) resembles particulate phosphorus (pP), chlorophyll, and other indicators of phytoplankton biomass. Very high pCo (>10 pM) was measured in the highly productive waters in the Peru upwelling ecosystem while lower concentrations (2–4 pM) were found in oligotrophic surface waters. West of 100° W, a secondary pCo maximum between 300–500 m overlaps with high particulate Mn

Biogeosciences Discuss., doi:10.5194/bg-2016-169, 2016
Manuscript under review for journal Biogeosciences
Published: 18 May 2016

(pMn), reflecting Co incorporation into Mn-oxides in oxygenated thermocline waters. Elevated pCo was also found at the top of the OMZ in the eastern half of the transect, corresponding with high dCo from remineralization. High pP and low pMn in these samples suggest that pCo may be present as biomass in anoxic bacterial and archaeal communities (Ohnemus et al., In Review), rather than incorporation into bacterial Mn-oxides by co-oxidation. pMn increases sharply west of 100° W, implying that pCo here is present as an authigenic phase (Fig. 9, Ohnemus et al., In Review; Moffett and Ho, 1996).

dCo can be bound by extremely strong organic ligands that affect its reactivity (Ellwood and van den Berg, 2001; Saito and Moffett, 2001). These ligands may be composed of degradation products of the cobalt-bearing cofactor vitamin B_{12} and may be stabilized following oxidation of Co(II) to Co(III) (Baars and Croot, 2014). Unlike other metals such as Fe, dCo bound to natural ligands is kinetically inert to ligand exchange (although some forms may still be bioavailable) and strong Co(II) ligands are not in excess of dCo, largely due to binding competition with nanomolar levels of labile nickel (Saito and Moffett, 2001; Saito et al., 2005). These properties can result in a significant fraction of labile dissolved cobalt (LCo) that can be measured without the UV-oxidation procedure necessary to measure dCo, especially in the mesopelagic (Noble et al., 2012).

On GP16, the distribution of LCo is similar to that of dCo (Figs. 3, 4, 6). Except for samples from the upper 50 m, dCo and LCo form a linear relationship (R^2 = 0.88) whose slope indicates that ~33 % of dCo is labile (Fig. 7a). Major exceptions are confined to the highly productive waters over the Peru shelf (Stations 1–6) where LCo is much lower than expected from dCo. In

Biogeosciences Discuss., doi:10.5194/bg-2016-169, 2016
Manuscript under review for journal Biogeosciences
Published: 18 May 2016

these waters, LCo decreases in step with silicate (Fig. 7c). As in the North and South Atlantic (Noble et al., 2012; Noble and Saito, in prep), LCo is undetectable in the surface ocean outside of the waters influenced by upwelling (beyond 100° W, Fig. 6b). The absence of LCo from the upper 300 m of the water column is deeper than corresponding gradients in the Atlantic, suggesting cobalt depletion is more intense in the South Pacific.

In the deep Pacific (>3000 m), where dCo is low, LCo is undetectable. LCo remains low (<15 pM) in the mesopelagic, except where the OMZ is most intense (Fig. 4). Within the OMZ, LCo maxima coincide with dCo maxima (Stations 1–15), but further to the west these LCo maxima are much less intense and occur deeper than dCo maxima (Fig. 3). The LCo plume from the OMZ extends deeper (below 2000 m) than the corresponding dCo (<2000 m), suggesting that remineralization and scavenging affect these quantities in different ways. Slight secondary maxima between 1500–2000 m (10–15 pM) appear in the center of the section on σ_θ = 27.7–8 kg m^{-3} isopycnal layers (Fig. 4c, 105° W–115° W), perhaps tracing transport of LCo remineralized in the eastern basin as these waters flow over the mid ocean ridge.

4. Discussion

4.1 Basin-scale coupling between dCo and O_2

The most striking aspect of the dCo distribution in the ETSP is the very high concentrations present in the OMZ (Figs. 3–5). Similar distributions have been observed in both the North and South Atlantic, where >100 pM dCo plumes corresponded to low oxygen waters underneath the Benguela and Mauritanian upwelling systems (Noble et al., 2012; Noble and Saito, in prep). In the North Pacific, profiles from the Costa Rica Dome (Ahlgren et al., 2014), the California

Biogeosciences Discuss., doi:10.5194/bg-2016-169, 2016
Manuscript under review for journal Biogeosciences
Published: 18 May 2016

margin (Biller and Bruland, 2013; Knauer et al., 1982), and the Central Pacific along 155° W (Saito et al., 2014) support an OMZ-cobalt plume there as well. Based on measurements from these four OMZs, oxygen biogeochemistry seems to exert a major control on cobalt cycling throughout the oceans.

Between the Atlantic and Pacific basins, the magnitude of the observed dCo plumes does not appear to scale with minimum O_2. While offshore O_2 in the Atlantic OMZs exceeds 20 µM, much of the ETSP is anoxic (Karstensen et al., 2008; Ulloa et al., 2012): Winkler titrations of discreet samples measured on the GP16 cruise indicate minimum O_2 to be <5 µM, while *in situ* sensors suggest true concentrations in the ETSP can be even lower (Thamdrup et al., 2012). Yet, dCo in the ETSP occupies a similar 100–200 pM range reported for the North and South Atlantic OMZs (Noble et al., 2012; Noble and Saito, in prep). Either the redox thresholds that affect processes like water column scavenging or sedimentary release are met in the suboxic Atlantic as well as the anoxic Pacific, or the apparent evenness in dCo concentration between OMZs results from other factors besides O_2 (e.g. continental sources, dust, remineralization).

In the ETSP, tight coupling between dCo and O_2 results in the strong inverse relationship that describes all samples below 200 m (Fig. 5a). In light of the nutrient-like dCo depletion in the surface of the ETSP and elsewhere (Fig. 6, Ahlgren et al., 2014; Dulaquais et al., 2014b; Noble et al., 2012), this negative correlation might be attributed to remineralization: dCo is returned to the dissolved phase from a sinking biogenic phase following respiration (i.e. O_2 consumption). The slope of the dCo:O_2 line (-0.33 µM M^{-1}, R^2 = 0.75 for 200–5500 m) might then represent the biological stoichiometry of the exported organic material in the ETSP. However, Co:P ratios in

Biogeosciences Discuss., doi:10.5194/bg-2016-169, 2016
Manuscript under review for journal Biogeosciences
Published: 18 May 2016

409 particulate material collected in the upper 50 m on GP16 indicate greater phytoplankton cobalt
410 utilization (median pCo:pP of 140 μM M^{-1} ÷ 118 O_2:P M M^{-1} = 1.2 Co:O_2 μM M^{-1}; Fig. 13C;
411 DeVries and Deutsch, 2014). If the dCo:O_2 trend is borne solely from remineralization, a greater
412 slope would be expected. The linearity in the dCo:O_2 relationship is also not reproduced upon
413 conversion of O_2 to apparent oxygen utilization (AOU = $O_{2,saturation} - O_{2,\ measured}$, Fig. 5b, R^2 =
414 0.49), implying that other factors besides remineralization (such as circulation and scavenging)
415 shape the subsurface dCo distribution as well.
416
417 In the deep ocean, near-conservative mixing of dCo with high and low O_2 water masses probably
418 contributes to the observed dCo:O_2 relationship. The enormous depth range (>5000 m) described
419 by the linear dCo:O_2 relationship contrasts with the near-exponential decrease in
420 remineralization rates with depth (e.g. Karstensen et al., 2008). It is likely that deep Pacific
421 circulation acts to spread signals of local dCo remineralization throughout the water column,
422 aggregating a multitude of export stoichiometries and remineralization processes into a single,
423 coherent relationship across the basin. LCo is undetectable below ~2500 m and the shallower
424 slope of the LCo:O_2 trend (-0.11 μM M^{-1}, R^2 = 0.67) implies that the dCo:O_2 relationship is
425 driven mostly by strongly complexed species, which are less vulnerable to co-oxidation by Mn-
426 oxidizing bacteria in the water column (Moffett and Ho, 1996). Since the deep Pacific can be
427 broadly regarded as a mixture of oxygenated circumpolar waters and OMZs (especially from the
428 North Pacific), the linear dCo:O_2 relationship between 200 and 5500 m may reflect mixing of a
429 dCo pool that is largely inert to losses by scavenging.
430

Biogeosciences Discuss., doi:10.5194/bg-2016-169, 2016
Manuscript under review for journal Biogeosciences
Published: 18 May 2016

In the upper 200 m, dCo is not well coupled with O_2 and almost all samples fall above the line established by deeper samples (Fig. 5a). Near the South American margin, the dCo maximum in the upper OMZ is more than double the 0 µM intercept of the dCo:O_2 relationship from deeper waters (77 pM, Fig. 5a). Given their resemblance to profiles of excess N_2 from denitrification (Chang et al., 2010), it is likely that both the dCo maximum and its decrease with depth are driven by a combination of remineralization of sinking biogenic cobalt and lateral transport of a coastal cobalt source (DeVries et al., 2012).

4.2 Distinct surface and mesopelagic Co:P relationships

In the upper ocean (0–200 m), dCo is linearly related to PO_4 (Figs. 5c and 7b), indicating that the processes controlling PO_4 in the surface – upwelling, mixing, biological uptake and export – are the main drivers of dCo as well. In the upper 50m, the dCo:PO_4 slope (69 µM:M, R^2 = 0.89, Fig. 7b) may describe export stoichiometry throughout the Eastern Pacific. That the surface dCo: PO_4 slope intercepts the highest dCo concentrations (below the 50 m depth range of the regression, Fig. 5c) indicates that new cobalt sourced from the shelf is rapidly incorporated into biological cycling and that the capacity for phytoplankton Co uptake is not overwhelmed by the order of magnitude higher dCo in coastal waters relative to the open ocean. Culture experiments with model diatoms and coccolithophores demonstrate this capacity (Shaked et al., 2006; Sunda and Huntsman, 1995; Yee and Morel, 1996), deploying Co to zinc enzymes to maintain activity when Zn becomes scarce. When Zn is limiting, Co quotas, as judged by open ocean phytoplankton (Sunda and Huntsman, 1992; Twining and Baines, 2013), are 10–100x greater than Co quotas when Zn is replete. Therefore, minor substitution of Zn quotas by Co (~10 %)

Biogeosciences Discuss., doi:10.5194/bg-2016-169, 2016
Manuscript under review for journal Biogeosciences
Published: 18 May 2016

453 can double cellular Co levels in eukaryotes, resulting in nearly complete uptake of dCo from the
454 surface ocean.
455
456 A separate nutrient-like dCo:PO_4 trend arises from gradients of both elements in the open ocean
457 nutricline (Fig. 5c). The slope of the mesopelagic trend (16 μM:M, for 200–1000 m, Figure 5c) is
458 much less than that measured for the upper 50 m (69 μM:M). Due to considerable preformed PO_4
459 in deep waters, as well as elevated dCo:PO_4 ratios in the OMZ, the mesopelagic dCo:PO_4
460 regression is considerably less robust than in the surface (R^2 = 0.21), though the slope does
461 reflect dCo and PO_4 covariation in this depth range when PO_4 < 2 μM (Fig. 5c). Regardless, there
462 seems to be a fundamental mismatch between dCo:PO_4 from the upper water column (0–200 m)
463 and that observed deeper (200–1000 m). In the eastern margin, the surface and mesopelagic
464 dCo:PO_4 vectors are joined at 2.6 μM PO_4 by a near-vertical line that makes the dCo:PO_4 domain
465 triangular. Interpretation of this line depends largely on its perceived direction: a downward
466 vector can be a fingerprint of scavenging while an upward vector describes a cobalt source
467 (Noble et al., 2008; Saito et al., 2010). This ambiguity is clarified by examining dCo:PO_4
468 gradients within isopycnal surfaces, which strongly indicate a source at low O_2. In the ETSP, σ_θ
469 26.2 and 26.4 isopycnals host the upper OMZ and the oxygenated thermocline waters west of
470 100° W. Water masses on these surfaces can be distinguished on the basis of salinity; from the
471 GP16 dataset, mixing between salty and deoxygenated equatorial sub-surface waters (ESSW or
472 13° C water) with fresher, ventilated Sub-Antarctic waters is apparent (Fiedler and Talley, 2006;
473 Toggweiler et al., 1991). Oxygenated waters on σ_θ = 26.2 and 26.4 show a tight coupling
474 between dCo and PO_4 (Fig. 8). For samples with < 20μM O_2, however, deviation from the oxic
475 dCo:PO_4 trend is always positive, indicating a dCo source within the OMZ. When oxygen is

Biogeosciences Discuss., doi:10.5194/bg-2016-169, 2016
Manuscript under review for journal Biogeosciences
Published: 18 May 2016

low, dCo follows salinity. Mixing of high salinity (34.9–35.0), high dCo ESSW from the northeast with low salinity, low dCo Subantarctic waters explains the dCo:salinity covariation on these isopycnal surfaces. While ESSW is fed by the lower equatorial undercurrent (EUC), which originates near Papua New Guinea and transports a large Fe and Al source eastward (Slemons et al., 2010), it is low in dCo (as measured at 155° W, Hawco and Saito, unpublished; Saito et al., 2014). When the EUC bifurcates near the Galapagos, it mixes with coastal waters north and south of the equator (Fiedler and Talley, 2006; Stramma et al., 2010), where its high dCo signature is likely acquired.

The isopycnal dCo:salinity relationship also implies cobalt scavenging in the OMZ is low. This is not surprising given the thermodynamic barriers to MnO_2 formation at low O_2 (Johnson et al., 1996; von Langen et al., 1997) and very low particulate Mn measured in the ETSP OMZ (Fig. 9). In the OMZ, both pCo:pP and pMn:pP ratios in the OMZ are consistent with micronutrient use by microbial communities and resemble biomass collected in the euphotic zone on GP16 (Co:P = 0.5–4 x 10^{-4} M M^{-1}, Mn:P ~10^{-3} M M^{-1}, Ohnemus et al., In Review). These low, biomass-like pCo:pP and pMn:pP signatures in the ETSP OMZ are consistent with redox-barriers to Mn oxidation at very low O_2 (Ohnemus et al., In Review).

Crossing the anoxic/oxic transition at 100° W in the thermocline (σ_θ 26.2–27.0, centered at 300 m) results in a factor of ten higher pMn concentrations and implies a redox threshold to Mn oxidation in the mesopelagic (Fig. 9). Heterotrophic Mn-oxidizing bacteria are known to incorporate Co by enzymatic co-oxidation into the Mn-oxide lattice and are prevalent throughout the water column (Cowen and Bruland, 1985; Moffett and Ho, 1996). While particulate Co

Biogeosciences Discuss., doi:10.5194/bg-2016-169, 2016
Manuscript under review for journal Biogeosciences
Published: 18 May 2016

profiles in the ETSP have a near-surface maximum from biological uptake (Fig. 7c), pCo attenuates much less with depth than pP in oxic thermocline waters. Very high pCo:pP ratios (up to 10^{-3} M M^{-1}) are found in the oxygenated thermocline but not in the OMZ (σ_θ 26.2–27.0, Fig. 9). The coincidence of high pCo:pP and high pMn throughout the in the mesopelagic is consistent with pCo being present in an authigenic Mn-oxide phase, marking an important transition between nutrient-like cobalt cycling in the surface ocean (where pCo is almost entirely biogenic) to Mn-oxide driven scavenging at depth.

The stimulation of cobalt scavenging across the anoxic/oxic transition at 100° W was reflected in a sharp decrease in LCo:PO_4 as scavenging removed LCo from the water column (Fig. 9). Indeed, the same oxygenated thermocline samples with high pMn and pCo:pP are responsible for the shallow vector in dCo:PO_4 space (16 μM M^{-1}, Fig. 5c). The offset between high surface and low mesopelagic dCo:PO_4 is mirrored by the lower surface and higher mesopelagic pCo:pP. While scavenging is often presumed to draw chiefly from metals in the dissolved phase, the heterotrophic nature of Mn-oxidizing bacteria and their abundance in sediment traps hint that Mn-oxidizing bacteria may access biogenic metal pools within sinking particles (Cowen and Bruland, 1985). In such a case, pCo may be shunted directly from a biogenic to an authigenic phase without being truly remineralized, preventing the equal return of dCo at depth relative to that exported from the surface, as documented here by the disparity between deep and shallow dCo:PO_4 slopes (Fig. 14). An important consequence of mesopelagic scavenging is that ventilation of these waters by upwelling without an exogenous source (e.g. margin sediments) would create conditions whereby dCo, relative to PO_4, is not supplied to the same extent it is presently utilized and exported. Because these scavenged waters are relatively shallow and have

Biogeosciences Discuss., doi:10.5194/bg-2016-169, 2016
Manuscript under review for journal Biogeosciences
Published: 18 May 2016

short ventilation ages (Fiedler and Talley, 2006), fluxes of cobalt to the South Pacific from margin sources must be sufficiently rapid to balance scavenging losses.

4.3 A major cobalt source from the Peruvian shelf

The strong covariation between high dCo and low O_2 in the ETSP and the intersection of the OMZ with the South American margin suggests that reducing sediments along the continental shelf may be an important cobalt source. Sections from the North and South Atlantic (Noble et al., 2012; Noble and Saito, in prep) and profiles from the North Pacific (Ahlgren et al., 2014; Knauer et al., 1982) have resulted in similar assertions, but the coincidence of high phytoplankton productivity along eastern margins also imprints signals from elevated remineralization. This is certainly the case for the ETSP, where stations 2 and 3 on the Peru shelf featured > 1.5 μg chlorophyll L^{-1} in the euphotic layer, and > 4 μM nitrite throughout the OMZ from intensified anoxic remineralization. As a result, all but one station along the shelf shows a dCo maximum at the oxycline, rather than the benthic boundary layer (Fig. 10). The lone exception, Station 2, is also the most shoreward, having respective dCo and LCo maxima of 159 pM and 59 pM at the deepest depth (110 m), indicating a flux of cobalt to the water column.

A survey of continental shelf sediments underlying the Peru OMZ found low Co/Al ratios (1.2 ± 0.3 x 10^{-4} g g^{-1}, Böning et al., 2004) relative to Andesitic and upper continental crusts (2.63 and 2.11 x 10^{-4} g g^{-1} respectively, McLennan, 2001; Taylor and McLennan, 1995), requiring that about half of the Co delivered to the continental shelf from crustal sources dissolved prior to burial on the shelf. The only other element to have a similar depletion was Mn, which covaried with Co across all samples in the Böning et al. study, consistent release of both metals by

Biogeosciences Discuss., doi:10.5194/bg-2016-169, 2016
Manuscript under review for journal Biogeosciences
Published: 18 May 2016

545 reductive dissolution. Near-surface Co and Mn content were slightly higher in the shallowest
546 sediments (<150 m water column depth) and uniformly low at deeper locations (Böning et al.,
547 2004), implying that sedimentation outpaces dissolution of Co and Mn only in very shallow
548 water columns and/or proximal to input, which explains the lack of dissolved benthic maxima for
549 both elements beyond Station 2 (Fig. 10).
550
551 Positive correlations between dCo, LCo and dMn within the OMZ on the Peru shelf reflect a
552 shared source (Figs. 10, 11). The slope of the LCo:dMn relationship, 18 ± 2 mM M^{-1} R^2 = 0.76,
553 is nearly identical to that in upper continental crust and Andesite (21–26 mM M^{-1}, McLennan,
554 2001; Taylor and McLennan, 1995), matching expectations that mineral dissolution should
555 provide should provide labile Co. However, the steeper slope for the dCo:dMn relationship (42 ±
556 5 mM M^{-1} R^2 = 0.67) exceeds crustal endmembers. Addition of a second, Co-enriched
557 component is needed to explain the observed relationship. Given the massive productivity over
558 the Peru shelf, biological export of dCo and dMn into the OMZ is a reasonable cause for the high
559 Co:Mn ratio in the shelf OMZ. From particulate material in the upper 40 m of shelf stations (1–
560 5), the Co:Mn ratio in biomass is 100–110 mM M^{-1} (median and mean), ~5 times higher than
561 crust, and falling within the range reported for single cell analysis of phytoplankton cells (70–
562 400 mM M^{-1}, Twining and Baines, 2013). The combination, then, of a high biotic Co:Mn and a
563 lower ratio from a sedimentary source can produce the slope observed in the water column, but
564 requires remineralized dCo to be chiefly ligand-bound in order to preserve the near-crustal
565 LCo:Mn slope. The higher phytoplankton Co:Mn ratio relative to their shared sedimentary
566 source results in a nutrient trap that returns upwelled dCo to the OMZ more efficiently than dMn
567 and implies that input of dCo from the shelf is rapidly followed by biological utilization,

Biogeosciences Discuss., doi:10.5194/bg-2016-169, 2016
Manuscript under review for journal Biogeosciences
Published: 18 May 2016

568 demonstrated in the transition from a dMn-like profile below the oxycline to a PO_4-like profile
569 above it (Fig. 10).
570
571 The Co/Al ratio in buried sediments on the continental shelf can provide a course measure of
572 how much Co has been released to the ocean. Sub-crustal Co/Al ratios in Peruvian sediments
573 between 9–14° S (Böning et al., 2004) match similar measurements in Chilean OMZ sediments
574 at 36° S (Co/Al = 1.3 ± 0.1 x 10^{-4} g g^{-1}, Table 2, Böning et al., 2009) and the Gulf of California
575 (1.4 x 10^{-4} g g^{-1}, Brumsack, 1989). The deficit between these values and continental crust (2.11 x
576 10^{-4} g g^{-1}) implies that dissolution of crustal materials along the eastern margin provides a large
577 source of dCo and LCo to the Pacific. Ultimately, this source is needed to balance extremely
578 high Co/Al ratios in Pacific pelagic sediments, which collect Co scavenged from the water
579 column (e.g Dunlea et al., 2015; Goldberg and Arrhenius, 1958).
580
581 In contrast to depleted Co along the South American shelf, Co/Al in shelf sediments from the
582 western margin of the Pacific appears crustal (Table 2). Holocene records from the Pearl River
583 delta and shelf slope in the South China Sea ~20° N (Hu et al., 2012, 2013) show mean Co/Al of
584 2.2 and 2.1 x 10^{-4} g g^{-1}, respectively, similar to sediments from the Gulf of Papua at 9° S (2.3 x
585 10^{-4} g g^{-1}, Alongi et al., 1996). Crustal Co/Al in these sedimentary systems implies that most of
586 the Co provided from fluvial sediment delivery either does not dissolve or is quickly reburied by
587 water column Mn oxidation, rates of which can be very high in estuaries and coastal seas
588 (Moffett and Ho, 1996; Moffett, 1994; Sunda and Huntsman, 1987; Sunda and Huntsman, 1990).
589

Biogeosciences Discuss., doi:10.5194/bg-2016-169, 2016
Manuscript under review for journal Biogeosciences
Published: 18 May 2016

590 It is likely that oxidizing conditions in the water column prevent reductive dissolution on the
591 western margin, leading to crustal Co/Al ratios in shelf sediments, while suboxic conditions on
592 the eastern margin mobilize Co, evident in depleted Co/Al ratios. Although sedimentary anoxia
593 releases Co bound in Mn oxides, even a thin layer of O_2 penetration into sediments results in a
594 near-zero diffusive flux into the water column (Heggie and Lewis, 1984). Bottom water
595 deoxygenation restores Co fluxes to the water column (Johnson et al., 1988, Sundby et al., 1986),
596 but Co sulfide minerals can also precipitate, analogous to 'Goldilocks' mechanisms for benthic
597 Fe release where flux is maximized when redox conditions are low enough to promote oxide
598 dissolution but still high enough to avoid pyrite burial (and by analogy, CoS; Scholz et al., 2014).
599 CoS burial is evident in high Co/Al content of Black Sea sediments (Brumsack, 2006) and
600 sulfide-rich pockets of Namibian sediments near Walvis Bay ($2.9 \pm 0.7 \times 10^{-4}$ g g^{-1}, Borchers et
601 al., 2005), despite more widespread Co/Al depletion in suboxic (but not sulfidic) terrigenous
602 sediments underneath the Benguela upwelling region (Bremner and Willis, 1993). Prevailing
603 suboxic conditions along the Namibian coast ultimately lead to extensive dCo, dMn, and dFe
604 plumes that reach across the South Atlantic basin (Noble et al., 2012). Similarly, depleted
605 sedimentary Co/Al on the Peruvian margin and high dCo in the water column perhaps reflect
606 sustained anoxia that, in the present, is unlikely outside the domain of OMZs.
607
608 Can a terrigenous cobalt source account for the observed OMZ plume? Because lithogenic
609 sediments along the Peru margin are delivered primarily by rivers (Scheidegger and Krissek,
610 1982), we can estimate a dCo flux to OMZ waters as the product of the fluvial sediment delivery
611 to the continental shelf and the difference in Co/Al ratios between original rocks and buried shelf
612 sediments:

Biogeosciences Discuss., doi:10.5194/bg-2016-169, 2016
Manuscript under review for journal Biogeosciences
Published: 18 May 2016

$$\text{Co flux}_{\text{suboxic}} = \left(\frac{\text{Co}}{\text{Al}}_{\text{crust}} - \frac{\text{Co}}{\text{Al}}_{\text{suboxic sediments}}\right) * \% \text{ Al} * \text{F}_{\text{fluvial}} \quad (1)$$

where $F_{fluvial}$ is the riverine flux of terrigenous sediments from Ecuador, Peru and Northern Chile to oxygen-depleted coastlines in the ETSP. If this supply is approximately 200 MT year^{-1} (Lyle, 1981; Milliman and Farnsworth, 2011), the Co deficit in Peruvian sediments from Böning et al., 2004 corresponds to a 2.5–4.6 x 10^7 mol per year flux from the South American shelf, depending on the crustal endmember applied. When scaled to the size of the ETSP OMZ (2.2 x 10^6 km^3 defined at 20µM, Fuenzalida et al., 2009) a terrigenous cobalt supply of 11–21 pM year^{-1} would be expected.

The extent to which the coastal flux and dCo inventory are in agreement depends on the residence time of OMZ waters. Models and CFC distributions from WOCE imply an approximately decadal recirculation time in OMZ waters relative to mesopelagic gyre circulation in the ETSP (Deutsch et al., 2001, 2011). Integrating our terrigenous Co flux estimate over 10 years yields an expected concentration of 120–230 pM within the OMZ. This is of similar magnitude, but greater than the concentrations measured on the GP16 transect (mean of 100 ± 30 pM). The difference between estimated and actual dCo inventories in the OMZ is probably due to upwelling and advection by surface currents, readily seen in the dCo section (Fig. 6), which carries the remainder to the gyre.

We can compare the calculated sedimentary flux to an expected flux from aerosol dust dissolution. Aeolian deposition is extremely low over the South Pacific basin (Mahowald et al., 2005), except immediately offshore of Peru, where dust from the Altiplano interacts with the prevailing northward winds (Prospero and Bonatti, 1969; Scheidegger and Krissek, 1982). Model

Biogeosciences Discuss., doi:10.5194/bg-2016-169, 2016
Manuscript under review for journal Biogeosciences
Published: 18 May 2016

results (Mahowald et al., 2005) suggest that deposition does not exceed 0.5 g m^{-2} yr^{-1}, except very close to the coastline. Using this estimate, crustal cobalt abundances, and the aerial extent of the OMZ (9.8 x 10^6 km^2, Fuenzalida et al., 2009), we can estimate an aerial flux of Co from dust to be 1.4 x 10^6 mol Co per year. A 10% fractional solubility for Co (Shelley et al., 2012) indicates a soluble cobalt flux from dust of 0.065 pM $year^{-1}$, ~0.5 % of the expected sedimentary flux. Over a decade, dust deposition accounts < 1 pM of the OMZ dCo plume. dCo profiles also lack surface maxima near shore despite corresponding features for dissolved Al and Mn at Stations 1 and 5 (Fig. 10, Resing et al., 2015). Fluvial sediment delivery to the margin, therefore, is a much more plausible source for the elevated dCo in the ETSP OMZ.

4.4 An inefficient cobalt source in hydrothermal vents

Hydrothermal venting along the Eastern Pacific Rise (EPR) provides a major source of dFe and dMn to the deep South Pacific (Resing et al., 2015) where nanomolar concentrations of both metals were measured between 2000–3000 m at the ridge crest and concentrations exceeded background values for several thousand kilometers westward. In contrast, dCo concentrations are only slightly elevated at the ridge crest (Station 18, Fig. 12), reaching 36 pM at 2400m (against a background of ~25 pM); at the same station, dFe and dMn both exceeded 15 nM (background <1 nM). Unambiguous hydrothermal input is evident from the LCo profile, which peaks at 14 pM at the dCo maximum (Fig. 12), roughly consistent with a 10,000-fold dilution of high temperature endmember sources containing 100–1000 nM dCo (Lupton et al., 1985; Metz and Trefry, 2000).

However, both dCo and LCo maxima are offset from dFe and dMn plumes. At station 18, dFe and dMn peak at 2500–2600 m. At this depth, LCo is undetectable and dCo values are at – or

Biogeosciences Discuss., doi:10.5194/bg-2016-169, 2016
Manuscript under review for journal Biogeosciences
Published: 18 May 2016

659 slightly lower than – background levels, suggesting that Mn and/or Fe scavenging in the heart of
660 the hydrothermal plume has removed most of the hydrothermal Co from the water column before
661 being transported away from the ridge crest (Fig. 12). Indeed, Co is strongly associated with Mn
662 phases in near-axis metalliferous sediment in the EPR at 14° S (Dunk and Mills, 2006). The
663 position of the LCo maximum above the dMn and dFe maxima probably reflects lower
664 scavenging rates outside the main plume, which may spare a fraction of the hydrothermal Co
665 source from an otherwise immediate and total removal. Even without scavenging losses, global
666 hydrothermal Co fluxes (2.2 Mmol $year^{-1}$; Swanner et al., 2014) are 10–25x less than our
667 estimated source from the Peru Shelf alone, highlighting the importance of upper ocean sources
668 in maintaining the dCo inventory.
669
670 **4.5 Cobalt scarcity in the euphotic zone**
671 The combination of eastern boundary upwelling and a continental source produces large dCo
672 gradients across the surface of the South Pacific Ocean (Fig. 13). Westward, decreasing surface
673 dCo results from phytoplankton uptake and export, reflected in strong correlations with PO_4, as
674 well as mixing with low dCo waters from the subtropical gyre. It is interesting to note that the
675 intercept for the dCo:PO_4 relationship is negative (-12.8 ± 2.6 μM M^{-1}, Fig. 7b); cobalt was
676 depleted before PO_4. This is opposite to what was observed in the Sargasso Sea, where extreme
677 PO_4 scarcity results in a positive dCo:PO_4 intercept (Jakuba et al., 2008). The dCo nutricline in
678 the South Pacific gyre (~200 m, Figs. 3, 6) is also deeper than corresponding features in the
679 North and South Atlantic (Noble et al., 2012; Noble and Saito, in prep). Because winter mixed
680 layers in the tropical South Pacific do not exceed 100 m and strong haloclines separate the
681 oxygen minimum layer from the surface (Fiedler and Talley, 2006), convective overturn does not

Biogeosciences Discuss., doi:10.5194/bg-2016-169, 2016
Manuscript under review for journal Biogeosciences
Published: 18 May 2016

682 reach the dCo nutricine at 150–250 m. Low vertical cobalt supply makes the South Pacific gyre
683 an interesting counterpoint to the Sargasso Sea, which experiences deep winter mixed layers and
684 higher dCo (10–30 pM, Dulaquais et al., 2014b; Jakuba et al., 2008; Noble and Saito, in prep),
685 and emphasizes the importance of lateral supply mechanisms, especially eastern boundary
686 upwelling, in maintaining the surface dCo inventory (Fig. 6, Saito et al., 2004).
687
688 While the South Pacific is thought to be limited by iron and nitrogen (Moore et al., 2013; Saito et
689 al., 2014), the extremely low dCo measured here implies that it may be important as well.
690 Because marine cyanobacteria such as *Prochlorococcus* and *Synechococcus* have an absolute Co
691 requirement (Saito et al., 2002; Sunda and Huntsman, 1995), they are vulnerable to limitation.
692 Indeed, a *Synechococcus* bloom in the Costa Rica Dome was found to be co-limited by both iron
693 and cobalt (Saito et al., 2005). Despite dCo concentrations below 10 pM (sometimes below the
694 3pM detection limit), the South Pacific gyre contains a significant *Prochlorococcus* population –
695 evident in the high proportion of divinyl chlorophyll A to total chlorophyll (Fig. 13b). As LCo
696 was undetectable beyond 100° W, biological uptake must occur either by accessing strongly
697 bound dCo or through fast cycling of LCo at very low steady-state concentrations. On GP16,
698 particulate Co concentrations in the upper 50 m were steady (3.5 ± 1.2 pM) and sometimes
699 equaled dissolved concentration. Compared to low pCo:dCo ratios observed in the South
700 Atlantic (<1:12, Noble et al., 2012), the high ratio in the South Pacific gyre (~1:3, Fig. 13a)
701 indicates that resident *Prochlorococcus* are extremely well-adapted to widespread dCo scarcity.
702
703 Unlike its near uniform relationship with dCo in the underlying OMZ, LCo measured on GP16 is
704 low relative to dCo in the surface ocean (0–50 m), especially along the Peru Margin (Fig. 6b,

Biogeosciences Discuss., doi:10.5194/bg-2016-169, 2016
Manuscript under review for journal Biogeosciences
Published: 18 May 2016

13c). This might result either from microbial production of cobalt ligands – as observed in a *Synechococcus*-dominated community in the Costa Rica Dome (Saito et al., 2005) – or if LCo is the preferred species for uptake. The latter has been demonstrated in culture with model eukaryotic algae (Sunda and Huntsman, 1995), where free Co ion is acquired by high affinity Zn-transporters. Because the Peru upwelling region is dominated by diatoms (Bruland et al., 2005), preferential uptake of free Co ion by these organisms is realistic and is corroborated by a strong correlation between LCo and dissolved silicate (Si) in the upper 50 m of the section (R^2 = 0.90). As a result of diatom-driven export, LCo in shelf surface waters is nearly depleted (1–12 pM) despite high concentrations of dCo (40–80 pM). Very low surface LCo at 12° S on GP16 contrasts with previous observations showing high concentrations of LCo in the Peru upwelling region during August–September 2000 (Saito et al., 2004). Between 5–10° S, much higher surface dCo was measured in freshly upwelled waters (up to 315 pM) and dCo was >50 % labile in surface transects (Saito et al., 2004). Surface dFe during August–September 2000 was also higher between 5–10° S than on GP16 at 12° S (Bruland et al., 2005; Resing et al., 2015). Decreasing surface dFe from North to South followed decreasing gradients in shelf width and fluvial sediment supply (Bruland et al., 2005; Milliman and Farnsworth, 2011), implying that the high dFe was due to stronger benthic sources to the North. Because coastal sources are expected to provide labile cobalt (e.g. Fig 11), the high concentrations of LCo measured between 5–10° S during August–September 2000 indicate a similar gradient in coastal dCo input and LCo availability in surface waters.

Spatial and temporal variability of margin dCo sources may ultimately affect carbon flow through the Peru upwelling ecosystem. Considering the very low dissolved Zn in surface waters

Biogeosciences Discuss., doi:10.5194/bg-2016-169, 2016
Manuscript under review for journal Biogeosciences
Published: 18 May 2016

on GP16 (<100 pM east of 90° W, S. John personal communication) and that >95 % of the dZn is typically complexed by organic ligands (Bruland, 1989), coastal diatoms off of Peru may be subject to diffusion limitation when free Zn ion falls below a 1–10 pM threshold (Sunda and Huntsman, 1992). Because Co can replace Zn in carbonic anhydrase enzymes (Sunda and Huntsman, 1995; Yee and Morel, 1996), LCo supplied from the margin may maintain fast rates of carbon fixation and export in the Peru Upwelling region despite low dZn. The relatively low concentrations measured on GP16, however, imply that the LCo supply may not always be sufficient.

5. Conclusions

The basin scale association between high dCo and low O_2 throughout the GP16 section testifies to the importance of redox chemistry and remineralization in maintaining the dCo distribution in the Eastern South Pacific (Fig. 14). High dCo and LCo on the Peru shelf match depleted Co content reported in Peru shelf sediments and indicate a large source to the water column (Böning et al., 2004). Correlations between dMn and LCo in anoxic shelf waters, and crust-like Co/Al ratios in oxic western boundary sediments suggest that margin cobalt sources are redox sensitive and that the sustained presence of the OMZ on the Peru margin amplifies coastal Co fluxes. Additionally, low oxygen in offshore OMZ waters suppresses particulate Mn accumulation and Co scavenging, evident in isopycnal dCo-salinity relationships. When mixing introduces sufficient O_2 to stabilize Mn oxides, high particulate Co:P ratios in the mesopelagic accompany 10-fold higher particulate Mn. Scavenging in mesopelagic waters limits the full return of Co to the dissolved phase during remineralization, resulting in low dissolved Co:P ratios relative to that exported from the euphotic zone (Fig. 14). Oxidative scavenging also seems to limit the flux of

Biogeosciences Discuss., doi:10.5194/bg-2016-169, 2016
Manuscript under review for journal Biogeosciences
Published: 18 May 2016

751 Co from hydrothermal venting over the East Pacific rise, further emphasizing the Peru margin as
752 the most important Co source to the South Pacific.
753
754 The high dCo within the OMZ also leads to a large flux to the surface ocean by upwelling along
755 the Peru margin, where it is readily accessed by phytoplankton. Strong correlations with
756 phosphate across the surface ocean emphasize its significance as a micronutrient. Preferential
757 uptake of LCo over the Peru shelf by diatoms generates a linear relationship with silicate and Co
758 may be critical to sustaining carbonic anhydrase activity and CO_2 fixation during blooms. Given
759 that deep nutriclines in the South Pacific Gyre limit dCo supply from vertical mixing outside of
760 the upwelling zone, phytoplankton Co nutrition depends largely on lateral supply from the
761 Eastern Margin.
762
763 Ultimately, the dCo inventory in the South Pacific – and its availability to surface phytoplankton
764 – may be changing considerably as the size and intensity of the OMZ fluctuate. Recent warming
765 and stratification appear to have expanded the volume of low oxygen waters in the tropics
766 (Stramma et al., 2008, 2010). As such, dCo inventories may increase as lower O_2 hinders
767 mesopelagic Mn oxide production and scavenging. However, decreased wind-driven upwelling
768 and carbon export may cause anoxic waters along the shelf to contract (Deutsch et al., 2011,
769 2014) and decrease the Co flux from coastal sediments. Changes in the dCo inventory then
770 depend on the relative redox sensitivities of the margin Co source versus offshore scavenging in
771 the mesopelagic, neither of which are well understood. Considering the 100–200 year residence
772 time of Co in the ocean (Saito and Moffett, 2002), feedbacks on the surface dCo supply may
773 manifest more quickly than for other nutrients and may alleviate or exacerbate any existing Co

Biogeosciences Discuss., doi:10.5194/bg-2016-169, 2016
Manuscript under review for journal Biogeosciences
Published: 18 May 2016

774 limitation. Improved definition of biological Co limitation thresholds and efforts to reconstruct
775 the Co cycle in past climates may resolve whether future changes in OMZ structure will have
776 meaningful impacts on phytoplankton nutrition in the coming century.
777
778 **Author Contributions**
779 NJH, DCO and JAR participated on the EPZT cruise. NJH measured dCo and LCo. JAR
780 measured dMn; DCO and BST measured particulate Co, Mn, and P. NJH and MAS prepared the
781 manuscript with contributions from all authors.
782
783 **Acknowledgements**
784 We thank the Captain and Crew of the RV *Thomas G. Thompson* and the entirety of the science
785 party aboard the GP16 cruise, especially chief scientists Jim Moffett and Chris German. We also
786 thank Claire Parker and Cheryl Zurbrick for enormous efforts in sample collection, Greg Cutter
787 and Geo Smith for operating the trace metal rosette and Tow-Fish, respectively, and Sara
788 Rauschenberg and Rob Sherrell for particle sampling. Susan Becker, Melissa Miller, and Rob
789 Palomares contributed nutrient, oxygen, and salinity data. The technical and logistical expertise
790 of Dawn Moran and Matt McIlvin is unparalleled. We appreciate the efforts of the
791 GEOTRACES office in coordinating the GP16 expedition and thank Luca Pini and Mike
792 Kubicsko of Metrohm Autolab for assistance with voltammetry. This is PMEL publication
793 #4475 and JISAO publication 2648. This work was funded by NSF awards OCE-1233733 to
794 MAS, OCE-1232814 to BST, and OCE-1237011 to JAR.
795
796

Biogeosciences Discuss., doi:10.5194/bg-2016-169, 2016
Manuscript under review for journal Biogeosciences
Published: 18 May 2016

References

Ahlgren, N. A., Noble, A., Patton, A. P., Roache-Johnson, K., Jackson, L., Robinson, D., McKay, C., Moore, L. R., Saito, M. A. and Rocap, G.: The unique trace metal and mixed layer conditions of the Costa Rica upwelling dome support a distinct and dense community of Synechococcus, Limnol. Oceanogr., 59(6), 2166–2184, doi:10.4319/lo.2014.59.6.2166, 2014.

Alongi, D. M., Boyle, S. G., Tirendi, F. and Payn, C.: Composition and Behaviour of Trace Metals in Post-oxic Sediments of the Gulf of Papua, Papua New Guinea, Estuar. Coast. Shelf Sci., 42(2), 197–211, doi:10.1006/ecss.1996.0015, 1996.

Baars, O. and Croot, P. L.: Dissolved cobalt speciation and reactivity in the eastern tropical North Atlantic, Mar. Chem., doi:10.1016/j.marchem.2014.10.006, 2014.

Baxter, L. a, Bobrowski, a, Bond, a M., Heath, G. a, Paul, R. L., Mrzljak, R. and Zarebski, J.: Electrochemical and spectroscopic investigation of the reduction of dimethylglyoxime at mercury electrodes in the presence of cobalt and nickel., Anal. Chem., 70(7), 1312–23, doi:10.1021/ac9703616, 1998.

Biller, D. V. and Bruland, K. W.: Sources and distributions of Mn, Fe, Co, Ni, Cu, Zn, and Cd relative to macronutrients along the central California coast during the spring and summer upwelling season, Mar. Chem., 155, 50–70, doi:10.1016/j.marchem.2013.06.003, 2013.

Böning, P., Brumsack, H.-J., Böttcher, M. E., Schnetger, B., Kriete, C., Kallmeyer, J. and Borchers, S. L.: Geochemistry of Peruvian near-surface sediments, Geochim. Cosmochim. Acta, 68(21), 4429–4451, doi:10.1016/j.gca.2004.04.027, 2004.

Böning, P., Brumsack, H.-J., Schnetger, B. and Grunwald, M.: Trace element signatures of Chilean upwelling sediments at ~36°S, Mar. Geol., 259(1-4), 112–121, doi:10.1016/j.margeo.2009.01.004, 2009.

Borchers, S. L., Schnetger, B., Böning, P. and Brumsack, H.-J.: Geochemical signatures of the Namibian diatom belt: Perennial upwelling and intermittent anoxia, Geochemistry, Geophys. Geosystems, 6(6), n/a–n/a, doi:10.1029/2004GC000886, 2005.

Bown, J., Boye, M., Baker, A., Duvieilbourg, E., Lacan, F., Le Moigne, F., Planchon, F., Speich, S. and Nelson, D. M.: The biogeochemical cycle of dissolved cobalt in the Atlantic and the Southern Ocean south off the coast of South Africa, Mar. Chem., 126(1-4), 193–206, doi:10.1016/j.marchem.2011.03.008, 2011.

Bown, J., Boye, M. and Nelson, D. M.: New insights on the role of organic speciation in the biogeochemical cycle of dissolved cobalt in the southeastern Atlantic and the Southern Ocean, Biogeosciences, 9(7), 2719–2736, doi:10.5194/bg-9-2719-2012, 2012.

Bremner, J. . and Willis, J. .: Mineralogy and geochemistry of the clay fraction of sediments from the Namibian continental margin and the adjacent hinterland, Mar. Geol., 115(1-2), 85–116, doi:10.1016/0025-3227(93)90076-8, 1993.

Bruland, K. W.: Complexation of zinc by natural organic ligands in the central North Pacific, Limnol. Oceanogr., 34(2), 269–285, doi:10.4319/lo.1989.34.2.0269, 1989.

Bruland, K. W. and Lohan, M. C.: Controls of Trace Metals in Seawater, Treatise Geochemistry Second Ed., 6, 23–47, doi:10.1016/B978-0-08-095975-7.00602-1, 2003.

837 Bruland, K. W., Rue, E. L., Smith, G. J. and DiTullio, G. R.: Iron, macronutrients and diatom
838 blooms in the Peru upwelling regime: brown and blue waters of Peru, Mar. Chem., 93(2-4), 81–
839 103, doi:10.1016/j.marchem.2004.06.011, 2005.

840 Brumsack, H. J.: Geochemistry of recent TOC-rich sediments from the Gulf of California and
841 the Black Sea, Geol. Rundschau, 78(3), 851–882, doi:10.1007/BF01829327, 1989.

842 Brumsack, H. J.: The trace metal content of recent organic carbon-rich sediments: Implications
843 for Cretaceous black shale formation, Palaeogeogr. Palaeoclimatol. Palaeoecol., 232(2-4), 344–
844 361, doi:10.1016/j.palaeo.2005.05.011, 2006.

845 Chang, B. X., Devol, A. H. and Emerson, S. R.: Denitrification and the nitrogen gas excess in the
846 eastern tropical South Pacific oxygen deficient zone, Deep Sea Res. Part I Oceanogr. Res. Pap.,
847 57(9), 1092–1101, doi:10.1016/j.dsr.2010.05.009, 2010.

848 Cowen, J. P. and Bruland, K. W.: Metal deposits associated with bacteria: implications for Fe
849 and Mn marine biogeochemistry, Deep Sea Res. Part A. Oceanogr. Res. Pap., 32(3), 253–272,
850 doi:10.1016/0198-0149(85)90078-0, 1985.

851 Cutter, G. A. and Bruland, K. W.: Rapid and noncontaminating sampling system for trace
852 elements in global ocean surveys, Limnol. Oceanogr. Methods, 10(6), 425–436,
853 doi:10.4319/lom.2012.10.425, 2012.

854 Deutsch, C., Gruber, N., Key, R. M., Sarmiento, J. L. and Ganachaud, A.: Denitrification and N
855 2 fixation in the Pacific Ocean, Global Biogeochem. Cycles, 15(2), 483–506,
856 doi:10.1029/2000GB001291, 2001.

857 Deutsch, C., Brix, H., Ito, T. and Thompson, L.: Climate-forced variability of ocean hypoxia,
858 Science (80-.)., 333(6040), 336–339, doi:10.1126/science.1202422, 2011.

859 Deutsch, C., Berelson, W., Thunell, R., Weber, T., Tems, C., McManus, J., Crusius, J., Ito, T.,
860 Baumgartner, T., Ferreira, V., Mey, J. and van Geen, A.: Centennial changes in North Pacific
861 anoxia linked to tropical trade winds, Science (80-.)., 345(6197), 665–668,
862 doi:10.1126/science.1252332, 2014.

863 DeVries, T. and Deutsch, C.: Large-scale variations in the stoichiometry of marine organic
864 matter respiration, Nat. Geosci., 7(November), 1–5, doi:10.1038/ngeo2300, 2014.

865 DeVries, T., Deutsch, C., Primeau, F., Chang, B. and Devol, A.: Global rates of water-column
866 denitrification derived from nitrogen gas measurements, Nat. Geosci., 5(8), 547–550,
867 doi:10.1038/ngeo1515, 2012.

868 Dulaquais, G., Boye, M., Middag, R., Owens, S., Puigcorbe, V., Buesseler, K., Masqué, P., de
869 Baar, H. J. W. and Carton, X.: Contrasting biogeochemical cycles of cobalt in the surface
870 western Atlantic Ocean, Global Biogeochem. Cycles, 28(12), 1387–1412,
871 doi:10.1002/2014GB004903, 2014a.

872 Dulaquais, G., Boye, M., Rijkenberg, M. J. a and Carton, X.: Physical and remineralization
873 processes govern the cobalt distribution in the deep western Atlantic Ocean, Biogeosciences,
874 11(6), 1561–1580, doi:10.5194/bg-11-1561-2014, 2014b.

875 Dunk, R. M. and Mills, R. A.: The impact of oxic alteration on plume-derived transition metals
876 in ridge flank sediments from the East Pacific Rise, Mar. Geol., 229(3-4), 133–157,
877 doi:10.1016/j.margeo.2006.03.007, 2006.

878 Dunlea, A. G., Murray, R. W. and Harris, R. N.: Cobalt-based age models of pelagic clay in the
879 South Pacific Gyre, 2015.

880 Ellwood, M. J. and van den Berg, C. M. .: Determination of organic complexation of cobalt in
881 seawater by cathodic stripping voltammetry, Mar. Chem., 75(1-2), 33–47, doi:10.1016/S0304-
882 4203(01)00024-X, 2001.

883 Fiedler, P. C. and Talley, L. D.: Hydrography of the eastern tropical Pacific: A review, Prog.
884 Oceanogr., 69(2-4), 143–180, doi:10.1016/j.pocean.2006.03.008, 2006.

885 Fuenzalida, R., Schneider, W., Garcés-Vargas, J., Bravo, L. and Lange, C.: Vertical and
886 horizontal extension of the oxygen minimum zone in the eastern South Pacific Ocean, Deep Sea
887 Res. Part II Top. Stud. Oceanogr., 56(16), 992–1003, doi:10.1016/j.dsr2.2008.11.001, 2009.

888 Gaillardet, J., Viers, J. and Dupré, B.: Trace Elements in River Waters, in Treatise on
889 Geochemistry, vol. 5, pp. 225–272, Elsevier., 2003.

890 Goldberg, E. D. and G.O.S., A.: Chemistry of Pacific pelagic sediments, Geochim. Cosmochim.
891 Acta, 13(2-3), 153–212, doi:10.1016/0016-7037(58)90046-2, 1958.

892 Heggie, D. and Lewis, T.: Cobalt in pore waters of marine sediments, Nature, 311(5985), 453–
893 455, doi:10.1038/311453a0, 1984.

894 Hu, D., Böning, P., Köhler, C. M., Hillier, S., Pressling, N., Wan, S., Brumsack, H. J. and Clift,
895 P. D.: Deep sea records of the continental weathering and erosion response to East Asian
896 monsoon intensification since 14ka in the South China Sea, Chem. Geol., 326-327, 1–18,
897 doi:10.1016/j.chemgeo.2012.07.024, 2012.

898 Hu, D., Clift, P. D., Boning, P., Hannigan, R., Hillier, S., Blusztajn, J., Wan, S. and Fuller, D. Q.:
899 Holocene evolution in weathering and erosion patterns in the Pearl River delta, Geochemistry,
900 Geophys. Geosystems, 14(7), 2349–2368, doi:10.1002/ggge.20166, 2013.

901 Jakuba, R. W., Moffett, J. W. and Dyhrman, S. T.: Evidence for the linked biogeochemical
902 cycling of zinc, cobalt, and phosphorus in the western North Atltic Ocean, Global Biogeochem.
903 Cycles, 22(4), 1–13, doi:10.1029/2007GB003119, 2008.

904 Johnson, K. S., Stout, P. M., Berelson, W. M. and Sakamoto-Arnold, C. M.: Cobalt and copper
905 distributions in the waters of Santa Monica Basin, California, Nature, 332(6164), 527–530,
906 doi:10.1038/332527a0, 1988.

907 Johnson, K. S., Coale, K. H., Berelson, W. M. and Michael Gordon, R.: On the formation of the
908 manganese maximum in the oxygen minimum, Geochim. Cosmochim. Acta, 60(8), 1291–1299,
909 doi:10.1016/0016-7037(96)00005-1, 1996.

910 Karstensen, J., Stramma, L. and Visbeck, M.: Oxygen minimum zones in the eastern tropical
911 Atlantic and Pacific oceans, Prog. Oceanogr., 77(4), 331–350,
912 doi:10.1016/j.pocean.2007.05.009, 2008.

913 Knauer, G. a., Martin, J. H. and Gordon, R. M.: Cobalt in north-east Pacific waters, Nature,
914 297(5861), 49–51, doi:10.1038/297049a0, 1982.

915 von Langen, P. J., Johnson, K. S., Coale, K. H. and Elrod, V. a.: Oxidation kinetics of
916 manganese (II) in seawater at nanomolar concentrations, Geochim. Cosmochim. Acta, 61(23),
917 4945–4954, doi:10.1016/S0016-7037(97)00355-4, 1997.

918 Lupton, J. E., Delaney, J. R., Johnson, H. P. and Tivey, M. K.: Entrainment and vertical transport

of deep-ocean water by buoyant hydrothermal plumes, Nature, 316(6029), 621–623, doi:10.1038/316621a0, 1985.

Lyle, M.: Formation and growth of ferromanganese oxides on the Nazca plate, GSA bulliten, 269–295, 1981.

Mahowald, N. M., Baker, A. R., Bergametti, G., Brooks, N., Duce, R. a., Jickells, T. D., Kubilay, N., Prospero, J. M. and Tegen, I.: Atmospheric global dust cycle and iron inputs to the ocean, Global Biogeochem. Cycles, 19(4), n/a–n/a, doi:10.1029/2004GB002402, 2005.

McLennan, S. M.: Relationships between the trace element composition of sedimentary rocks and upper continental crust, Geochemistry, Geophys. Geosystems, 2(4), n/a–n/a, doi:10.1029/2000GC000109, 2001.

Metz, S. and Trefry, J. H.: Chemical and mineralogical influences on concentrations of trace metals in hydrothermal fluids, Geochim. Cosmochim. Acta, 64(13), 2267–2279, doi:10.1016/S0016-7037(00)00354-9, 2000.

Milliman, J. D. and Farnsworth, K. L.: River Discharge to the Coastal Ocean, Cambridge University Press, Cambridge., 2011.

Moffett, J. W.: A radiotracer study of cerium and manganese uptake onto suspended particles in Chesapeake Bay, Geochim. Cosmochim. Acta, 58(2), 695–703, doi:10.1016/0016-7037(94)90499-5, 1994.

Moffett, J. W. and Ho, J.: Oxidation of cobalt and manganese in seawater via a common microbially catalyzed pathway, Geochim. Cosmochim. Acta, 60(18), 3415–3424, doi:10.1016/0016-7037(96)00176-7, 1996.

Moore, C. M., Mills, M. M., Arrigo, K. R., Berman-Frank, I., Bopp, L., Boyd, P. W., Galbraith, E. D., Geider, R. J., Guieu, C., Jaccard, S. L., Jickells, T. D., La Roche, J., Lenton, T. M., Mahowald, N. M., Marañón, E., Marinov, I., Moore, J. K., Nakatsuka, T., Oschlies, A., Saito, M. a, Thingstad, T. F., Tsuda, A. and Ulloa, O.: Processes and patterns of oceanic nutrient limitation, Nat. Geosci., 6(9), 701–710, doi:10.1038/ngeo1765, 2013.

Noble, A. E. and Saito, M. A.: Total Dissolved Cobalt and Cobalt Speciation from the US North Atlantic GEOTRACES Zonal Transect, In Prep.

Noble, A. E., Saito, M. A., Maiti, K. and Benitez-Nelson, C. R.: Cobalt, manganese, and iron near the Hawaiian Islands: A potential concentrating mechanism for cobalt within a cyclonic eddy and implications for the hybrid-type trace metals, Deep Sea Res. Part II Top. Stud. Oceanogr., 55(10-13), 1473–1490, doi:10.1016/j.dsr2.2008.02.010, 2008.

Noble, A. E., Lamborg, C. H., Ohnemus, D. C., Lam, P. J., Goepfert, T. J., Measures, C. I., Frame, C. H., Casciotti, K. L., DiTullio, G. R., Jennings, J. and Saito, M. A.: Basin-scale inputs of cobalt, iron, and manganese from the Benguela-Angola front to the South Atlantic Ocean, Limnol. Oceanogr., 57(4), 989–1010, doi:10.4319/lo.2012.57.4.0989, 2012.

Ohnemus, D., Rauschenberg, S., Cutter, G. A. and Twining, B. S.: Elevated trace metal content of prokaryotic plankton communities associated with anoxic marine zones, Limnol. Ocean., In Review.

Price, N. M., Harrison, G. I., Hering, J. G., Hudson, R. J., Nirel, P. M. V., Palenik, B. and Morel, F. M. M.: Preparation and Chemistry of the Artificial Algal Culture Medium Aquil, Biol. Oceanogr., 6(5-6), 443–461, doi:10.1080/01965581.1988.10749544, 1989.

961 Prospero, J. M. and Bonatti, E.: Continental dust in the atmosphere of the Eastern Equatorial
962 Pacific, J. Geophys. Res., 74(13), 3362–3371, doi:10.1029/JC074i013p03362, 1969.

963 Resing, J. A., Sedwick, P. N., German, C. R., Jenkins, W. J., Moffett, J. W., Sohst, B. M. and
964 Tagliabue, A.: Basin-scale transport of hydrothermal dissolved metals across the South Pacific
965 Ocean, Nature, 523(7559), 200–203, doi:10.1038/nature14577, 2015.

966 Saito, M. A. and Moffett, J. W.: Complexation of cobalt by natural organic ligands in the
967 Sargasso Sea as determined by a new high-sensitivity electrochemical cobalt speciation method
968 suitable for open ocean work, Mar. Chem., 75(1-2), 49–68, doi:10.1016/S0304-4203(01)00025-
969 1, 2001.

970 Saito, M. A. and Moffett, J. W.: Temporal and spatial variability of cobalt in the Atlantic Ocean,
971 Geochim. Cosmochim. Acta, 66(11), 1943–1953, doi:10.1016/S0016-7037(02)00829-3, 2002.

972 Saito, M. A., Moffett, J. W., Chisholm, S. W. and Waterbury, J. B.: Cobalt limitation and uptake
973 in Prochlorococcus, Limnol. Oceanogr., 47(6), 1629–1636, doi:10.4319/lo.2002.47.6.1629,
974 2002.

975 Saito, M. A., Moffett, J. W. and DiTullio, G. R.: Cobalt and nickel in the Peru upwelling region:
976 A major flux of labile cobalt utilized as a micronutrient, Global Biogeochem. Cycles, 18(4), n/a–
977 n/a, doi:10.1029/2003GB002216, 2004.

978 Saito, M. A., Rocap, G. and Moffett, J. W.: Production of cobalt binding ligands in a
979 Synechococcus feature at the Costa Rica upwelling dome, Limnol. Oceanogr., 50(1), 279–290,
980 doi:10.4319/lo.2005.50.1.0279, 2005.

981 Saito, M. A., Goepfert, T. J., Noble, A. E., Bertrand, E. M., Sedwick, P. N. and DiTullio, G. R.:
982 A seasonal study of dissolved cobalt in the Ross Sea, Antarctica: micronutrient behavior,
983 absence of scavenging, and relationships with Zn, Cd, and P, Biogeosciences, 7(12), 4059–4082,
984 doi:10.5194/bg-7-4059-2010, 2010.

985 Saito, M. A., McIlvin, M. R., Moran, D. M., Goepfert, T. J., DiTullio, G. R., Post, A. F. and
986 Lamborg, C. H.: Multiple nutrient stresses at intersecting Pacific Ocean biomes detected by
987 protein biomarkers, Science (80-.)., 345(6201), 1173–1177, doi:10.1126/science.1256450, 2014.

988 Sarmiento, J. L., Gruber, N., Brzezinski, M. a and Dunne, J. P.: High-latitude controls of
989 thermocline nutrients and low latitude biological productivity, Nature, 479(7374), 556–556,
990 doi:10.1038/nature10605, 2011.

991 Scheidegger, K. F. and Krissek, L. A.: Dispersal and deposition of eolian and fluvial sediments
992 off Peru and northern Chile, Geol. Soc. Am. Bull., 93(2), 150, doi:10.1130/0016-
993 7606(1982)93<150:DADOEA>2.0.CO;2, 1982.

994 Scholz, F., McManus, J., Mix, A. C., Hensen, C. and Schneider, R. R.: The impact of ocean
995 deoxygenation on iron release from continental margin sediments, Nat. Geosci., 7(May), 433–
996 437, doi:10.1038/ngeo2162, 2014.

997 Shaked, Y., Xu, Y., Leblanc, K. and Morel, F. M. M.: Zinc availability and alkaline phosphatase
998 activity in Emiliania huxleyi: Implications for Zn-P co-limitation in the ocean, Limnol.
999 Oceanogr., 51(1), 299–309, doi:10.4319/lo.2006.51.1.0299, 2006.

1000 Shelley, R. U., Sedwick, P. N., Bibby, T. S., Cabedo-Sanz, P., Church, T. M., Johnson, R. J.,
1001 Macey, A. I., Marsay, C. M., Sholkovitz, E. R., Ussher, S. J., Worsfold, P. J. and Lohan, M. C.:
1002 Controls on dissolved cobalt in surface waters of the Sargasso Sea: Comparisons with iron and

aluminum, Global Biogeochem. Cycles, 26(2), n/a–n/a, doi:10.1029/2011GB004155, 2012.

Slemons, L. O., Murray, J. W., Resing, J., Paul, B. and Dutrieux, P.: Western Pacific coastal sources of iron, manganese, and aluminum to the Equatorial Undercurrent, Global Biogeochem. Cycles, 24(3), n/a–n/a, doi:10.1029/2009GB003693, 2010.

Stramma, L., Johnson, G. C., Sprintall, J. and Mohrholz, V.: Expanding Oxygen-Minimum Zones in the Tropical Oceans, Science (80-.)., 320(5876), 655–658, doi:10.1126/science.1153847, 2008.

Stramma, L., Johnson, G. C., Firing, E. and Schmidtko, S.: Eastern Pacific oxygen minimum zones: Supply paths and multidecadal changes, J. Geophys. Res., 115(C9), C09011, doi:10.1029/2009JC005976, 2010.

Sunda, W. G. and Huntsman: Diel cycles in microbial manganese oxidation and manganese redox speciation in coastal waters of the Bahama Islands, Limnol. Oceanogr., 35(2), 325–338, doi:10.4319/lo.1990.35.2.0325, 1990.

Sunda, W. G. and Huntsman, S. A.: Microbial oxidation of manganese in a North Carolina estuary, Limnol. Oceanogr., 32(3), 552–564, doi:10.4319/lo.1987.32.3.0552, 1987.

Sunda, W. G. and Huntsman, S. A.: Feedback interactions between zinc and phytoplankton in seawater, Limnol. Oceanogr., 37(1), 25–40, doi:10.4319/lo.1992.37.1.0025, 1992.

Sunda, W. G. and Huntsman, S. A.: Cobalt and zinc interreplacement in marine phytoplankton: Biological and geochemical implications, Limnol. Oceanogr., 40(8), 1404–1417, doi:10.4319/lo.1995.40.8.1404, 1995.

Sundby, B., Anderson, L. G., Hall, P. O. J., Iverfeldt, Å., van der Loeff, M. M. R. and Westerlund, S. F. G.: The effect of oxygen on release and uptake of cobalt, manganese, iron and phosphate at the sediment-water interface, Geochim. Cosmochim. Acta, 50(6), 1281–1288, doi:10.1016/0016-7037(86)90411-4, 1986.

Swanner, E. D., Planavsky, N. J., Lalonde, S. V., Robbins, L. J., Bekker, A., Rouxel, O. J., Saito, M. A., Kappler, A., Mojzsis, S. J. and Konhauser, K. O.: Cobalt and marine redox evolution, Earth Planet. Sci. Lett., 390, 253–263, doi:10.1016/j.epsl.2014.01.001, 2014.

Taylor, S. R. and McLennan, S. M.: The geochemical evolution of the continental crust, Rev. Geophys., 33(2), 241, doi:10.1029/95RG00262, 1995.

Thamdrup, B., Dalsgaard, T. and Revsbech, N. P.: Widespread functional anoxia in the oxygen minimum zone of the Eastern South Pacific, Deep Sea Res. Part I Oceanogr. Res. Pap., 65, 36–45, doi:10.1016/j.dsr.2012.03.001, 2012.

Toggweiler, J. R., Dixon, K. and Broecker, W. S.: The Peru upwelling and the ventilation of the south Pacific thermocline, J. Geophys. Res., 96(C11), 20467, doi:10.1029/91JC02063, 1991.

Tovar-Sánchez, A., Sañudo-Wilhelmy, S. a. and Flegal, A. R.: Temporal and spatial variations in the biogeochemical cycling of cobalt in two urban estuaries: Hudson River Estuary and San Francisco Bay, Estuar. Coast. Shelf Sci., 60(4), 717–728, doi:10.1016/j.ecss.2004.03.010, 2004.

Twining, B. S. and Baines, S. B.: The Trace Metal Composition of Marine Phytoplankton, Ann. Rev. Mar. Sci., 5(1), 191–215, doi:10.1146/annurev-marine-121211-172322, 2013.

Ulloa, O., Canfield, D. E., DeLong, E. F., Letelier, R. M. and Stewart, F. J.: Microbial oceanography of anoxic oxygen minimum zones., Proc. Natl. Acad. Sci. U. S. A., 109(40),

1044 15996–6003, doi:10.1073/pnas.1205009109, 2012.

1045 Yee, D. and Morel, F. M. M.: In vivo substitution of zinc by cobalt in carbonic anhydrase of a
1046 marine diatom, Limnol. Oceanogr., 41(3), 573–577, doi:10.4319/lo.1996.41.3.0573, 1996.

1047

1048

1049

1050 **Table 1.** Blanks and standards used during analyses.

		Co, pM	+/-	n	Consensus
At sea	Blank	3.7	1.2	28	
Oct – Dec,	Lab SW	4.5	2.1	28	
2013	D1	48.5	2.4	3	46.6 +/- 4.8
At WHOI,	Blank	4.7	1.4	12	
Sept – Nov,	GSP	2.5	2.0	10	4.9 +/- 1.2**
2014	D2	45.0	2.7	7	46.9 +/- 3.0
	GSC	77.7	2.4	4	***

1051 *Collected from South Pacific surface seawater Nov. 2011

1052 **Refers to SAFe standard S, which was collected at the same location

1053 ***No consensus

1054

1055

1056 **Table 2.** Co/Al ratios in sediments from different redox regimes.

Location	Co / Al x 10^{-4} (g g^{-1})		Reference
Crust			
Upper continental crust	2.11		McLennan 2001
Andesitic crust	2.63		Taylor and McLennan 1995
Eastern Boundary sediments			
Peru Upwelling Sediments	1.2 ± 0.3	9–14° S	Boning et al. 2004
Chile upwelling Sediments	1.3 ± 0.1	36° S	Boning et al. 2009
Gulf of California	1.4		Brumsack 1989
Namibian Shelf	1.0 ± 0.3	17–25° S, 'Terrigenous'	Bremner and Willis 1993
Sulfidic Sediments			
Namibian diatom belt	2.9 ± 0.7	Near Walvis Bay, 22.5° S	Borchers et al. 2005
Black Sea	3.8–6.2		Brumsack 2006
Western Boundary Sediments			
Papua New Guinea	2.3	8° S, Gulf of Papua	Alongi et al. 1996
Pearl River Delta	2.2 ± 0.4	22° N, (10–0 ka)	Hu et al. 2013
South China Sea Shelf Slope	2.1 ± 0.2	20° N, 2037m (14–0 ka)	Hu et al. 2012
Deep Ocean Sediments			
South Pacific Gyre	35 (2.9–101)	22° S–32° S, 100–0 Ma	Dunlea et al. 2015
Pelagic Pacific	17 (2–58)	50° N–20° S	Goldberg and Arrhenius 1958

1057

1058

Biogeosciences Discuss., doi:10.5194/bg-2016-169, 2016
Manuscript under review for journal Biogeosciences
Published: 18 May 2016

Figure Captions

Figure 1. The GP16 transect in the tropical South Pacific. Red circles indicate sampling stations. Dissolved oxygen from WOCE is plotted in blue and 10 μM contours are shown between 0–60 μM O_2. Station number increases sequentially westward, with the exception of Station 1.

Figure 2. Signal processing of voltammetry scans. Varying instrumental noise imprinted negative current excursions during measurement and necessitated data smoothing to correctly integrate the $Co(DMG)_2$ reduction peak at -1.15 V. For mild (a) and moderate (b) noise levels, a 2^{nd} order, 17-point smoothing was applied (red line, 97 % of scans). Increases in noise caused this routine to overestimate peak height (c) and a first order, 13-point smoothing was applied instead (~3 % of scans, blue line).

Figure 3. Profiles of dissolved cobalt (dCo, closed circles), labile cobalt (LCo, open circles) and O_2 (grey lines) across the South Pacific. Upper panels show a 0–1000 m depth range; bottom panel show full profiles. dCo and LCo are highest close to the Peru Margin (Station 1) and decrease westward. O_2 follows the opposite trend. The small peak at 2400 m at Station 18 shows peak hydrothermal input from the East Pacific Rise. Note that the dCo and LCo scales in the upper panel are adjusted to highlight gradients and differ from the lower panels.

Figure 4. Dissolved oxygen (a), dissolved cobalt (b) and labile cobalt (c) sections along GP16, projected on a longitudinal axis. Note high dCo and LCo stem from the Peru margin and overlap with the low O_2. Interpolations were made using Ocean Data View with DIVA gridding, with

Biogeosciences Discuss., doi:10.5194/bg-2016-169, 2016
Manuscript under review for journal Biogeosciences
Published: 18 May 2016

negative gridded values suppressed. The signal to noise ratio was set to 15 for dissolved and labile cobalt. Signal to noise for O_2 was set to the default, 50.

Figure 5. Coupling between dissolved cobalt with O_2 (a), AOU (b), and PO_4 (c). Below 200 m (red circles), dCo shows a decreasing linear trend with dissolved oxygen that is obscured upon conversion of O_2 to apparent oxygen utilization, AOU, and a weak relationship with PO_4. In the upper 200 m (blue circles), dCo and PO_4 are strongly coupled but dCo shows no relationship with O_2 or AOU. Trend lines in (c) show best fit for 0–50 m in particulate Co:P (146 μM M^{-1}, dotted line), 0–50 m dissolved Co:P (69 μM M^{-1}, blue line, see Fig. 7b) and 200–1000 m regression for dissolved Co:P (16 μM M^{-1}, red line). Processes affecting these plots are described in vector legends.

Figure 6. Dissolved cobalt (a), labile cobalt (b), and particulate cobalt (c) gradients in the upper 500 m of the ETSP. White lines in both panels show dissolved PO_4 contours at 0.5 μM increments. Interpolation was conducted using weight averaged gridding with 40 and 46 ‰ length scales in the x and y direction, respectively.

Figure 7. (a) The relationship between dissolved cobalt (dCo) and labile cobalt (LCo) in the South Pacific. LCo increases linearly with dCo with a slope of 0.33 (black dots), except for the upper 50 m (red dots), where samples fall below this trend due to preferential depletion of LCo by phytoplankton. (b) In the 0–50 m range, dCo strongly correlates with phosphate (R^2 = 0.89). (c) LCo is preferentially removed from surface waters (0–50 m) and tracks silicate (R^2 = 0.90).

Biogeosciences Discuss., doi:10.5194/bg-2016-169, 2016
Manuscript under review for journal Biogeosciences
Published: 18 May 2016

1104 **Figure 8**. Transition in dCo cycling at the OMZ boundary in the upper South Pacific
1105 thermocline. (a) Isopycnal windows centered at σ_θ = 26.2 ± 0.1 kg m^{-3} (circles) and σ_θ = 26.4 ±
1106 0.1 kg m^{-3} (triangles) show PO_4-coupled cycling in oxygenated waters (blue) but not in OMZ
1107 waters with O_2<20 μM (red). (b) In the OMZ, dCo follows salinity, indicating mixing between a
1108 high dCo endmember at a salinity of 35.0 and a fresher water mass that is low in dCo.
1109
1110 **Figure 9**. Redox control of Co and Mn scavenging. Within mesopelagic waters (σ_θ = 26.2–27.0
1111 kg m^{-3}, mean depth of 300 m), high O_2 in ventilating water masses result in a sharp redox
1112 boundary at the edge of the OMZ (red circles, scale in μM). Particulate Mn (pMn) increases
1113 across the oxic/anoxic boundary at 100° W (blue circles, in nM) and imply stabilization of Mn
1114 oxides. Both pMn:pP and pCo:pP (cyan and pink circles, respectively; units are M M^{-1}) increase
1115 across the OMZ boundary, exceeding predicted values from remineralization of biogenic
1116 material from the surface ocean (1.26 x 10^{-3} mean pMn:pP and 1.57 x 10^{-4} pCo:pP for 0–50 m
1117 (M M^{-1}), cyan and pink lines, respectively). Dissolved phase dCo:dPO_4 (black circles) and
1118 LCo:PO_4 (white circles) also decrease west of the OMZ boundary show scavenging of the dCo
1119 and LCo in the mesopelagic (units are M M^{-1}).
1120
1121 **Figure 10.** Profiles of dissolved cobalt (dCo, black), PO_4 (red) and dMn (blue) over the Peru
1122 shelf at 12° S. The oxycline (grey bar, defined by the first sample where O_2<10 μM) marks the
1123 transition between the OMZ and oxygenated surface waters. Station 2 is the closest to the coast.
1124 Note the similarity between dCo and PO_4 above the oxycline and the transition to a dMn-like
1125 profile beneath it.
1126

Biogeosciences Discuss., doi:10.5194/bg-2016-169, 2016
Manuscript under review for journal Biogeosciences
Published: 18 May 2016

Figure 11. Cobalt and Mn in the Peru shelf OMZ (GP16 Stations 1–5, O_2<20 uM). Dissolved cobalt (dCo, closed circled) and labile cobalt (LCo, white) follow positive linear relationships with dMn. The LCo slope (18 mM M^{-1}) approximates the Co:Mn ratio in upper continental crust and Andesite (red and pink lines 21 and 26 mM M^{-1}, respectively), suggesting it derives from a shelf source. The mean pCo:pMn ratio from phytoplankton dominated particles collected in the upper 40 m over the shelf (blue line, 105 mM M^{-1}) is greater than dCo:dMn slope (42 mM M^{-1}), indicating that dCo and dMn concentrations in the Peru shelf OMZ represent a combination of biomass remineralization and sedimentary input.

Figure 12. (a) Dissolved cobalt (dCo, black circles) and labile cobalt (LCo, white) in the East Pacific Rise hydrothermal plume. Profiles are from Station 18 at the EPR ridge crest at 113 °W. (b) dMn (blue lines) and dFe profiles (red) replotted from Resing et al. 2015 clearly show hydrothermal input. Grey shading below 2250 m indicates area of hydrothermal influence where dFe and dMn are >1 nM.

Figure 13. (a) The particulate to dissolved ratio of cobalt (pCo:dCo, in M M^{-1}, pink circles) in near-surface samples (0–50m) measured on GP16; a value of 1 indicates equal concentrations in each phase. (b) The ratio of divinyl chlorophyll A to total chlorophyll (green circles), a proxy for *Prochlorococcus* abundance. (c) The near-surface distribution of dissolved cobalt (dCo, black circles) and labile cobalt (LCo, white circles), showing higher concentrations near the Peru margin (<80° W) and very low dCo to the west.

Biogeosciences Discuss., doi:10.5194/bg-2016-169, 2016
Manuscript under review for journal Biogeosciences
Published: 18 May 2016

1149 **Figure 14.** A schematic cross-section of the cobalt cycle in the Eastern Tropical South Pacific.
1150 Black arrows describe idealized physical circulation, showing upwelling near the Peru margin,
1151 advection westward and subduction in the South Pacific gyre. Biological Co export is shown in
1152 the red-hashed arrows, and solid and dashed red arrows show remineralization and scavenging
1153 respectively. The margin source is shown as a red-outlined arrow. These vectors are also plotted
1154 on idealized oxygen and phosphate axes, using the same color scheme, to show how these
1155 processes appear in Co:O_2 and Co:PO_4 space.

Biogeosciences Discuss., doi:10.5194/bg-2016-169, 2016
Manuscript under review for journal Biogeosciences
Published: 18 May 2016

Figure 1

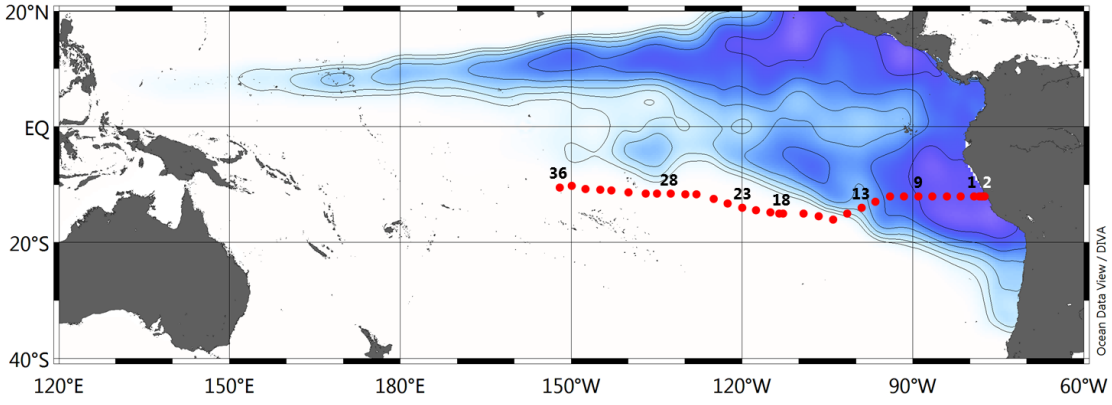

Biogeosciences Discuss., doi:10.5194/bg-2016-169, 2016
Manuscript under review for journal Biogeosciences
Published: 18 May 2016

Biogeosciences Discussions
Open Access
EGU

Figure 2

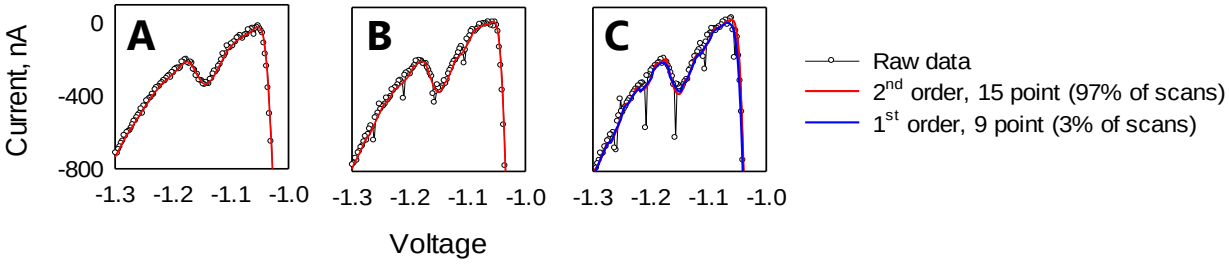

Biogeosciences Discuss., doi:10.5194/bg-2016-169, 2016
Manuscript under review for journal Biogeosciences
Published: 18 May 2016

Biogeosciences Discussions
Open Access
EGU

Figure 3

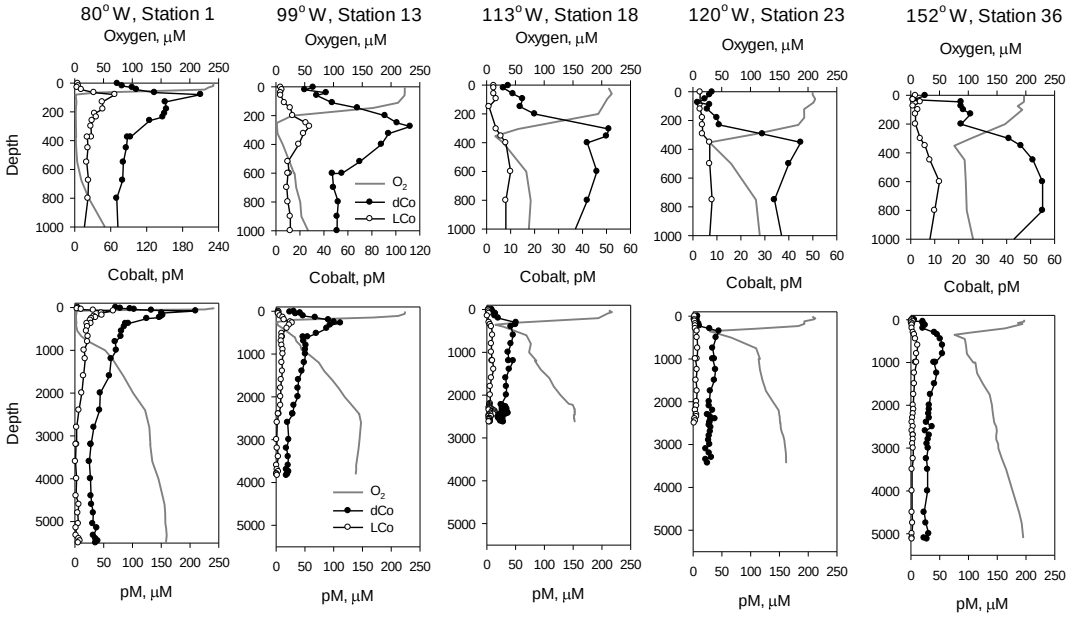

Biogeosciences Discuss., doi:10.5194/bg-2016-169, 2016
Manuscript under review for journal Biogeosciences
Published: 18 May 2016

Figure 4

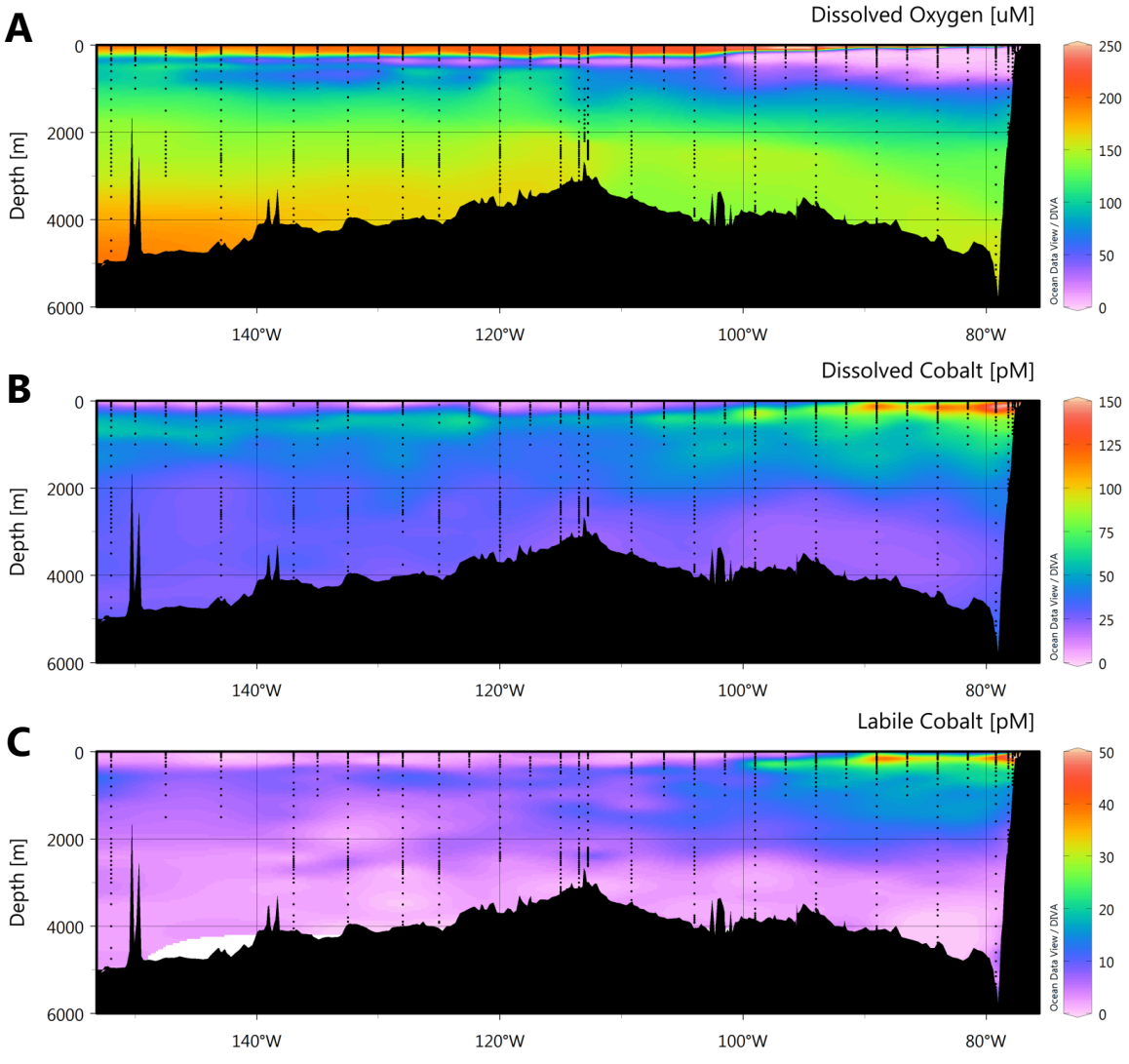

Biogeosciences Discuss., doi:10.5194/bg-2016-169, 2016
Manuscript under review for journal Biogeosciences
Published: 18 May 2016

Biogeosciences Discussions
Open Access
EGU

Figure 5

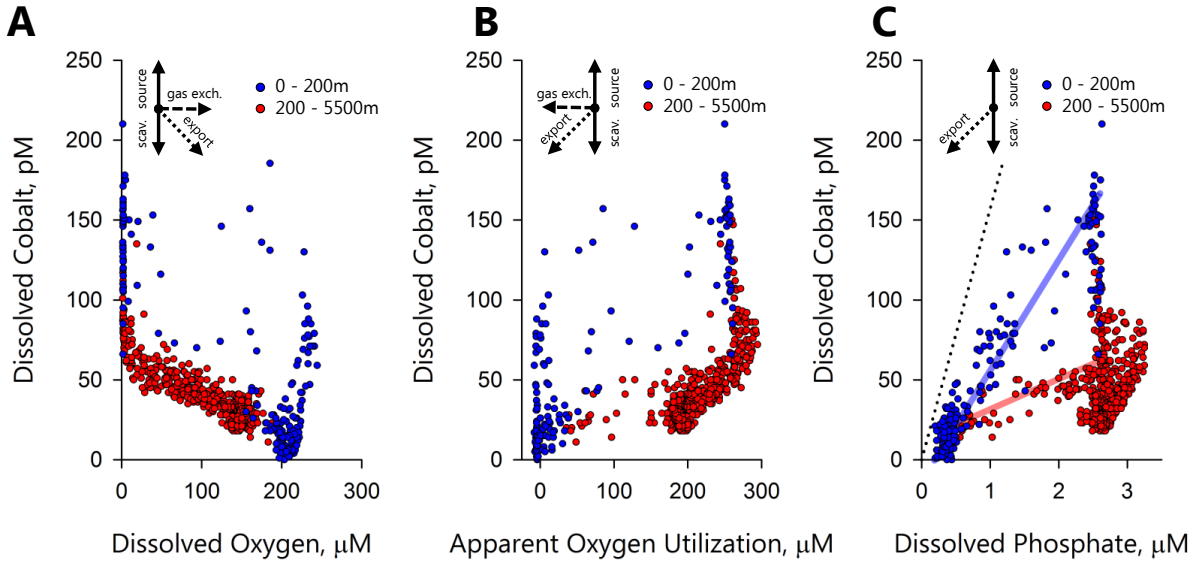

Biogeosciences Discuss., doi:10.5194/bg-2016-169, 2016
Manuscript under review for journal Biogeosciences
Published: 18 May 2016

Figure 6

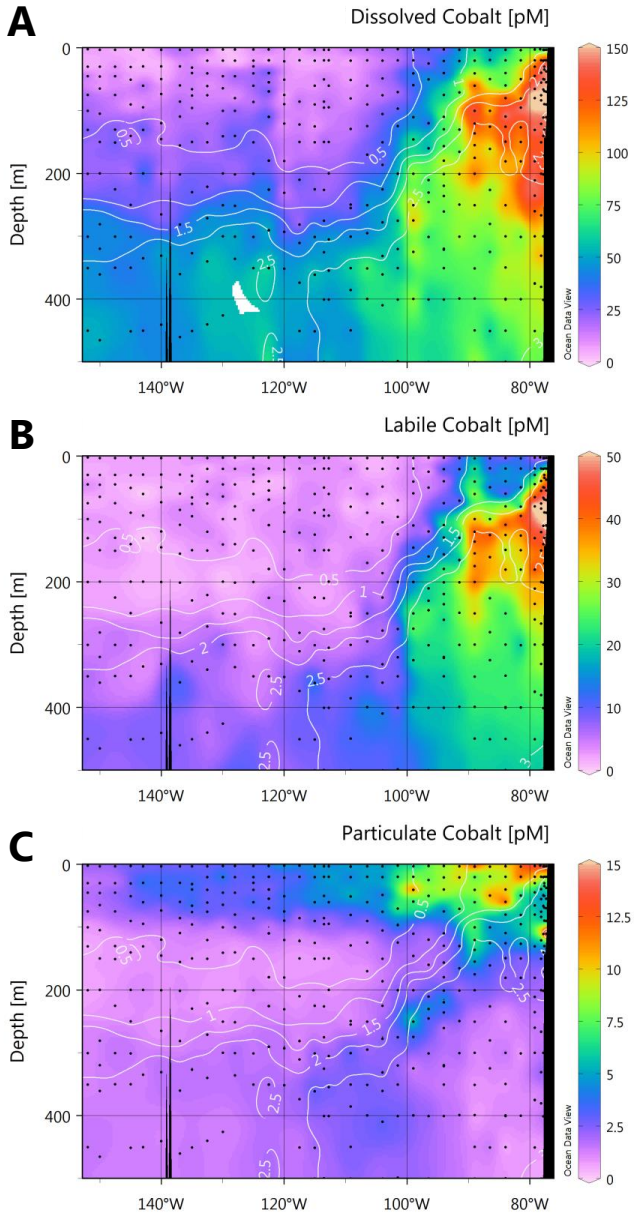

Biogeosciences Discuss., doi:10.5194/bg-2016-169, 2016
Manuscript under review for journal Biogeosciences
Published: 18 May 2016

Biogeosciences Discussions
Open Access
EGU

Figure 7

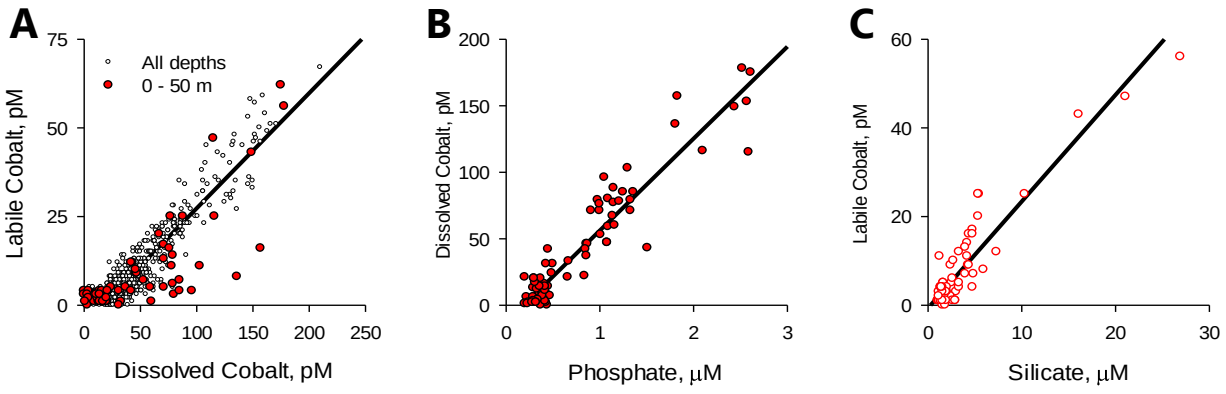

Biogeosciences Discuss., doi:10.5194/bg-2016-169, 2016
Manuscript under review for journal Biogeosciences
Published: 18 May 2016

Figure 8

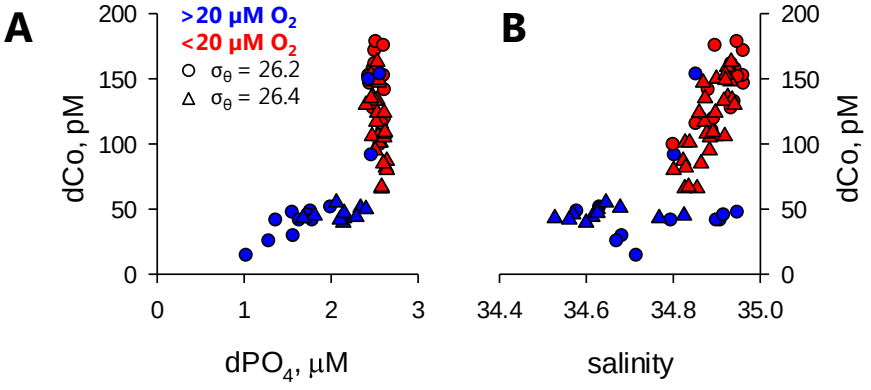

Biogeosciences Discuss., doi:10.5194/bg-2016-169, 2016
Manuscript under review for journal Biogeosciences
Published: 18 May 2016

Figure 9

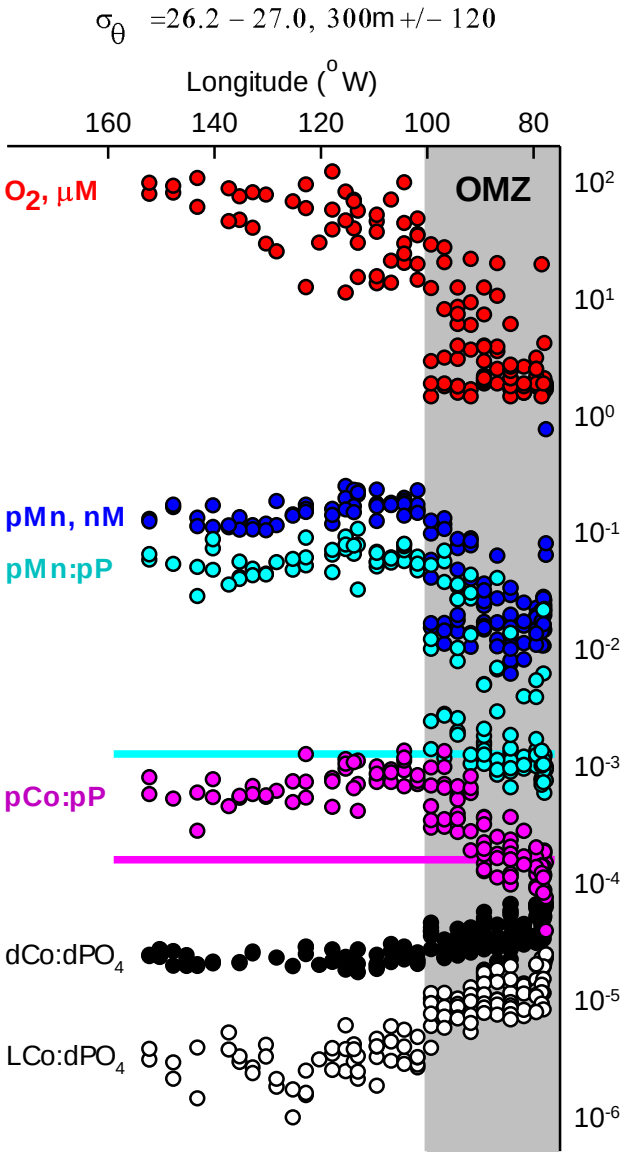

Biogeosciences Discuss., doi:10.5194/bg-2016-169, 2016
Manuscript under review for journal Biogeosciences
Published: 18 May 2016

Figure 10

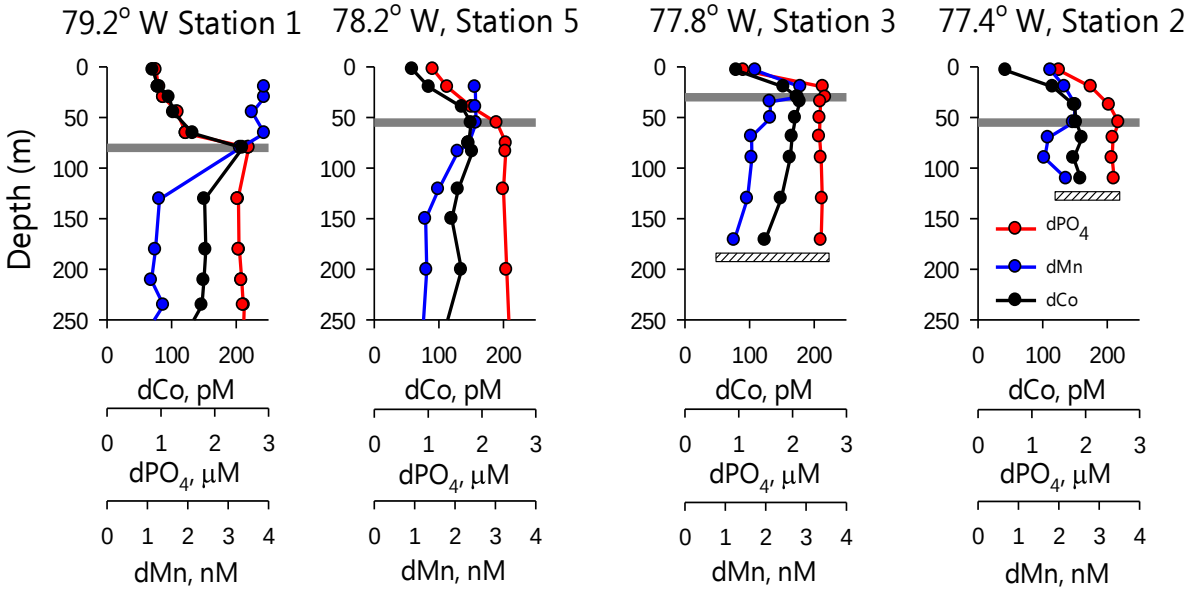

Biogeosciences Discuss., doi:10.5194/bg-2016-169, 2016
Manuscript under review for journal Biogeosciences
Published: 18 May 2016

Figure 11

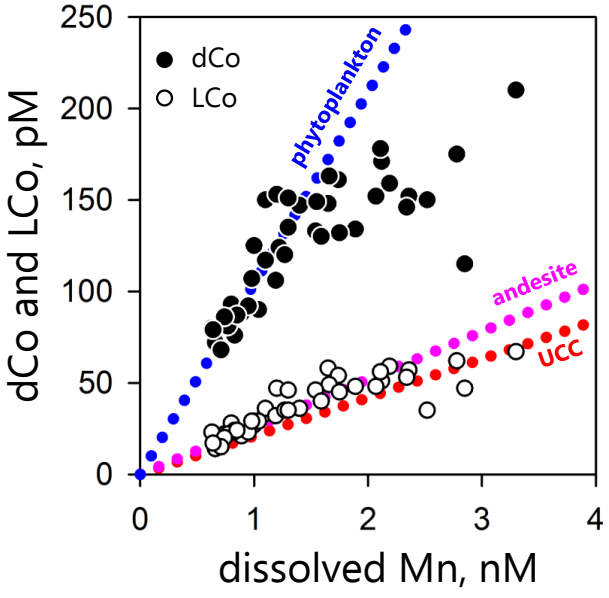

Biogeosciences Discuss., doi:10.5194/bg-2016-169, 2016
Manuscript under review for journal Biogeosciences
Published: 18 May 2016

Figure 12

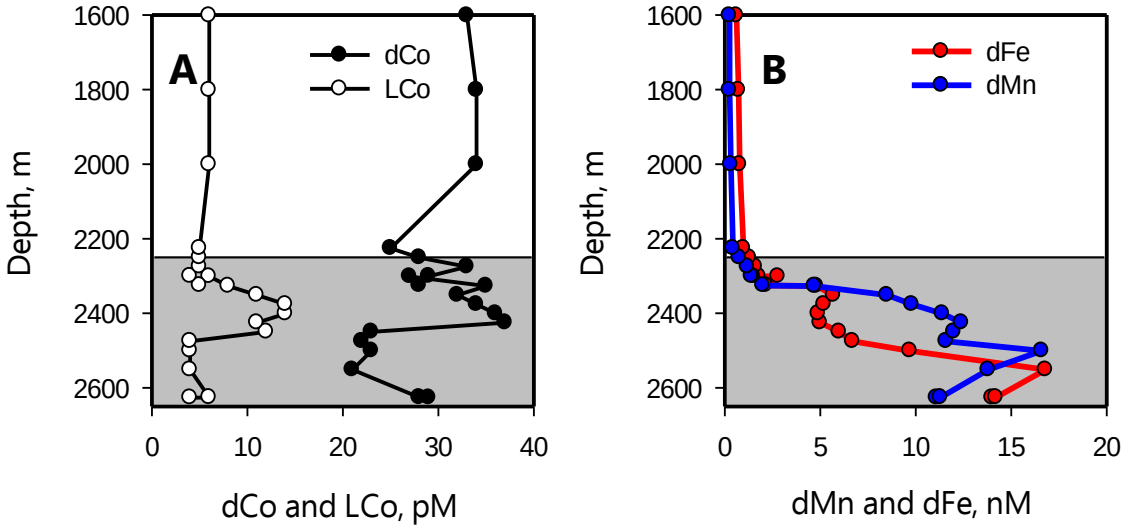

Biogeosciences Discuss., doi:10.5194/bg-2016-169, 2016
Manuscript under review for journal Biogeosciences
Published: 18 May 2016

Figure 13

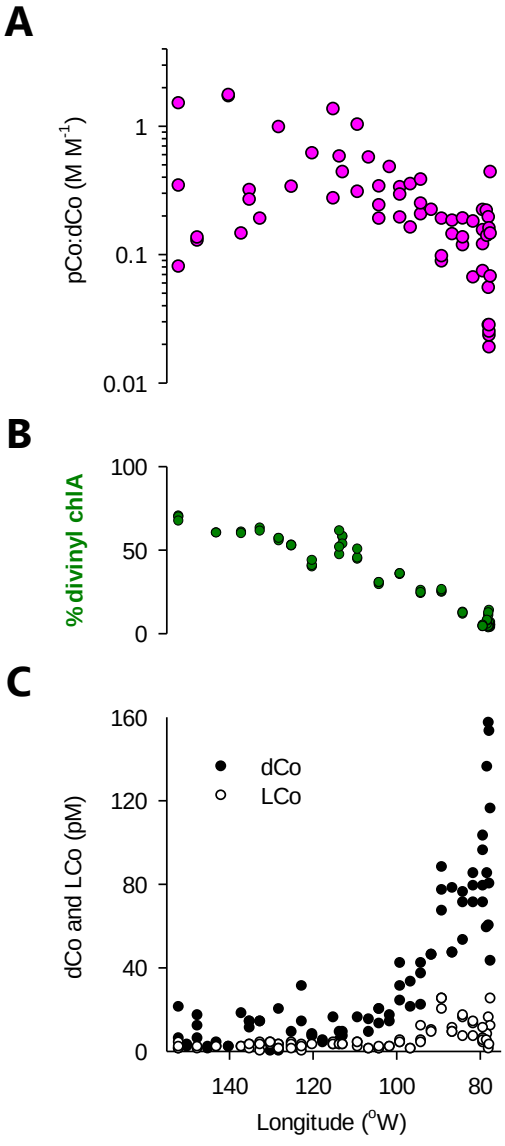

Biogeosciences Discuss., doi:10.5194/bg-2016-169, 2016
Manuscript under review for journal Biogeosciences
Published: 18 May 2016

Figure 14